



HAL
open science

Homochiral SCM Built of Tetrahedral and Pentagonal Bipyramidal Fe(II) Units Bridged by Chlorine

Valentin Jubault, Barthélémy Pradines, Céline Pichon, Nicolas Suaud, Carine Duhayon, Nathalie Guihéry, Jean-Pascal Sutter

► **To cite this version:**

Valentin Jubault, Barthélémy Pradines, Céline Pichon, Nicolas Suaud, Carine Duhayon, et al.. Homochiral SCM Built of Tetrahedral and Pentagonal Bipyramidal Fe(II) Units Bridged by Chlorine. *Crystal Growth & Design*, 2023, 23 (2), pp.1229-1237. 10.1021/acs.cgd.2c01360 . hal-03981782

HAL Id: hal-03981782

<https://hal.science/hal-03981782>

Submitted on 10 Feb 2023

HAL is a multi-disciplinary open access archive for the deposit and dissemination of scientific research documents, whether they are published or not. The documents may come from teaching and research institutions in France or abroad, or from public or private research centers.

L'archive ouverte pluridisciplinaire **HAL**, est destinée au dépôt et à la diffusion de documents scientifiques de niveau recherche, publiés ou non, émanant des établissements d'enseignement et de recherche français ou étrangers, des laboratoires publics ou privés.

Homochiral SCM built of tetrahedral and pentagonal bipyramidal Fe(II) units bridged by chlorine

Valentin Jubault,^a Barthélémy Pradines,^b Céline Pichon,^{a,*} Nicolas Suaud,^{b,*} Carine Duhayon,^a Nathalie Guihéry,^{b,*} Jean-Pascal Sutter^{a,*}

^a Laboratoire de Chimie de Coordination du CNRS (LCC), Université de Toulouse, CNRS, F-31077 Toulouse, France.

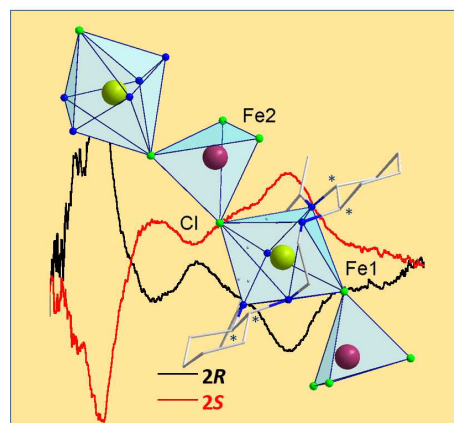
e-mail : jean-pascal.sutter@lcc-toulouse.fr ; celine.pichon@lcc-toulouse.fr

^b Laboratoire de Chimie et Physique Quantiques (LCPQ), Université de Toulouse, CNRS, 118 route de Narbonne, F-31062 Toulouse, France.

e-mail: suaud@irsamc.ups-tlse.fr ; nathalie.guihery@irsamc.ups-tlse.fr

Abstract

Each enantiomer of a chiral pentagonal bipyramidal (PBP) Fe^{II} complex ([FeL^{N5R,R}Cl(MeOH)]Cl·H₂O, **1R**, or [FeL^{N5S,S}Cl(MeOH)]Cl·H₂O, **1S**.) have been obtained using either the *R* or the *S* stereoisomer of the macrocyclic pentadentate ligand formed in a template-condensation reaction of the tetraamine N,N'-Bis-((1*R*,2*R*)-[2-(amino)]cyclohexyl)-1,2-diaminoethane, or its (1*S*,2*S*) enantiomer, and 2,5-diacetylpyridine, respectively L^{N5R,R} and L^{N5S,S}. Subsequently, the 1-D coordination polymers [FeL^{N5R,R}{FeCl₄}], **2R**, and [FeL^{N5S,S}{FeCl₄}], **2S**, were formed by reacting respectively **1R** or **1S** with one equivalent of FeCl₂(H₂O)₄. These chain compounds consist in an alternation of PBP and tetrahedral Fe^{II} units sharing a chlorine atom.



These chain compounds consist in an alternation of PBP and tetrahedral Fe^{II} units sharing a chlorine atom. Theoretical calculations reveal large magnetic anisotropy for each Fe center but of different type with axial zero-field splitting parameter *D* of respectively -30 cm⁻¹ and 15 cm⁻¹. The magnetic behavior for the 1-D compound revealed canted antiferromagnetic Fe-Fe interactions (*J* = -6 cm⁻¹) and SCM behavior characterized by $\Delta/k_B = 42$ K with pre-exponential factor $\tau_0 = 2.17 \times 10^{-10}$ s. It was noted that this SCM behavior was accompanied by a magnetic order leading to a weak-ferromagnet (*i.e.* canted antiferromagnet). The preparations, crystal structures (CCDC references 2214580 to 2214583), spectroscopic data, magnetic behaviors, and theoretical investigations are reported.

INTRODUCTION

Single-Chain Magnets (SCM) are one-dimensional coordination compounds belonging to the molecular nano-magnets.¹ They are characterized by a blocking of their magnetization whose relaxation is thermally activated and regulated by an energy barrier, Δ , as described by the Arrhenius equation.²⁻⁴ This magnetic behavior is intimately related to an overall easy-axis magnetic anisotropy and to a correlation energy resulting from exchange interactions between the individual paramagnetic centers of the 1D array. In addition to intensive work to achieve high blocking temperatures, an emerging interest concerns nano-magnets with a synergistic effect between the magnetic property and a second physical property; an effect that would be associated with the blocking of magnetization. A typical case of such synergy is the interaction between light and magnetism which leads to magneto-optical effects. A well-known example is magneto-chiral dichroism⁵ that becomes enhanced by a magnetic ordering⁶⁻⁸ but in all cases its observation was subjected to strong applied magnetic fields.⁹ ¹⁰ Circular polarized luminescence (CPL)¹¹ can also be a magneto-optical effect induced by the intrinsic magnetic field of a ferromagnetic material.¹² CPL has been observed for a luminescent single-molecule magnet (SMM) where it appeared in the same temperature range as the slow relaxation of the magnetization.¹³ The observation of such magneto-optical effect requires chiral compounds.

From a chemical perspective, the design based on the building block approach allows a rational implementation of the magnetic anisotropy and exchange interactions that will operate in the SCM.¹⁴ ¹⁵ In this perspective, metal complexes with pentagonal bipyramidal (PBP) coordination sphere have emerged as attractive units. This polyhedron shape gives access to a controlled magnetic anisotropy whose magnitude and sign are determined by the chosen metal ion.¹⁶ Moreover, when this coordination sphere is maintained by a pentadentate ligand localized in the equatorial sites, the structural robustness of these complexes allows chemical substitution of the apical positions without altering the magnetic anisotropy.¹⁷ These features have been used to obtain SCMs involving Fe^{II} or Ni^{II} PBP centers as a source of Ising-type anisotropy.¹⁸⁻²³

Following this approach, we report here the development of a chiral SCM derived from a PBP Fe^{II} complex based on an enantiopure macrocyclic pentadentate ligand. The 1-D coordination polymer consists of alternating PBP and pseudo-tetrahedral [FeCl₄]²⁻ units bridged by Cl-atoms. Depending on the enantiomer involved, it was possible to specifically obtain either stereoisomers of the supramolecular organization. For this 1-D coordination polymer, a canted antiferromagnetic ordering with SCM behavior was observed.

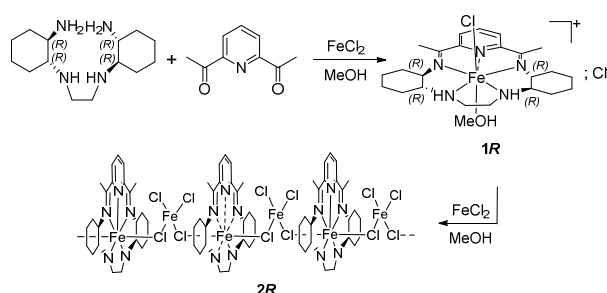
RESULTS AND DISCUSSION

Syntheses

The chiral macrocyclic ligands selected for this investigation results for the condensation of the tetraamine N,N'-Bis-((1*R*,2*R*)-[2-(amino)]cyclohexyl)-1,2-diaminoethane, or its (1*S*,2*S*) enantiomer, and 2,5-diacetylpyridine, respectively L^{N5*R*,*R*} and L^{N5*S*,*S*} (Scheme 1). This ligand was chosen because of the proximity of the asymmetric centers to the metal ion. It was known to lead to a PBP coordination sphere for Mn^{II},²⁴ and since a penta-aza ligand is also suitable to stabilize a PBP coordination sphere for Fe^{II},^{18, 25, 26} L^{N5*R*,*R*} and L^{N5*S*,*S*} appeared adapted to our aim. The ligand was actually formed in a template reaction with FeCl₂ to give the respective PBP Fe^{II} complex [FeL^{N5*R*,*R*}Cl(MeOH)]Cl·H₂O, **1R**, or

$[\text{FeL}^{\text{N5},\text{S}}\text{Cl}(\text{MeOH})]\text{Cl}\cdot\text{H}_2\text{O}$, **1S**. However, it appeared that the sequence of addition of the different ingredients had a significant effect on the result. When FeCl_2 was first reacted with diacetylpyridine and then tetra-amine was added, **1R** (or **1S**) formed in high yield, whereas reversing the addition sequence of the ligand constituents led to a mixture of products. The 1-D coordination polymers $[\text{FeL}^{\text{N5R},\text{R}}\{\text{FeCl}_4\}]$, **2R**, and $[\text{FeL}^{\text{N5S},\text{S}}\{\text{FeCl}_4\}]$, **2S**, were efficiently obtained reacting respectively **1R** or **1S** with one equivalent of $\text{FeCl}_2\cdot 4\text{H}_2\text{O}$.

Both **1R/S** and **2R/S** were readily obtained as crystalline blue solids (see experimental section) which allowed establishing their crystal structures and confirming the phase purity of the bulk samples by PXRD (Figure S1).



Scheme 1. Synthesis pathways for the preparation of $[\text{FeL}^{\text{N5R},\text{R}}\text{Cl}(\text{MeOH})]\text{Cl}\cdot\text{H}_2\text{O}$, **1R**, and the chain compound $[\text{FeL}^{\text{N5}}\{\text{FeCl}_4\}]$, **2R**. The same procedures apply for **1S** and **2S** with tetra-amine enantiomer (**1S**,**2S**).

Crystal structures

The crystal structures of the four compounds have been investigated. Because, apart from stereochemistry, they are equivalent two by two, only the *R* enantiomers will be described here. Crystal data, ORTEP plots of the asymmetric unit, and selected metric data for all the derivatives can be found in the Supporting Information (SI).

$[\text{FeL}^{\text{N5R},\text{R}}\text{Cl}(\text{MeOH})]\text{Cl}\cdot\text{H}_2\text{O}$, **1R**, crystallized in the space group $P2_12_12_1$. It consists in a heptacoordinated Fe^{II} complex (Figure 1) comprising a pentadentate macrocyclic ligand occupying the equatorial positions of the coordination polyhedron, while the apical positions are occupied by a methanol molecule and a chloride atom. The molecular complex is cationic and its charge is compensated by a chloride anion located outside the coordination sphere. The asymmetric unit is completed by a co-crystallized H_2O molecule. In the macrocycle the asymmetric carbons of the cyclohexyl groups are of *R* configuration, in agreement with the stereochemistry of the reagent, and two new centers of chirality are present. They are located on the N3 and N4 nitrogen atoms and result from the blocking of the inversion of these secondary amines by their coordination to the metal center. They are of *S* configuration which is induced by the adjacent chiral *R*-carbon atoms; in the related **1S** these chiral amines have *R* configuration (see Figure S2). The steric hindrance between the methyl groups and the cyclohexyl moieties leads in a slight twist of the macrocycle ligand in the equatorial plane with one methyl pointing up and one pointing down. The metal-ligand bond lengths of the first coordination sphere are given in the caption to Figure 1. The Fe^{II} ion is slightly eccentric to the center of the pentadentate ligand, being closer to the pyridine nitrogen (N1) than to the other nitrogen atoms. The N3 nitrogen is slightly below the equatorial plane as shown by the N3-Fe1-O1 angle of 83.02° . The whole forms a coordination sphere of slightly distorted PBP geometry. The deformation of the

coordination polyhedron with respect to the possible seven-apex geometries was evaluated through the CShM (Continuous Shape Measures) parameter determined with the program SHAPE.^{27, 28} The smallest deformation parameter was found for the pentagonal bipyramidal geometry with 0.49 for **1R**, and 0.54 for **1S** (Table S2) confirming a distorted PBP coordination sphere.²⁹

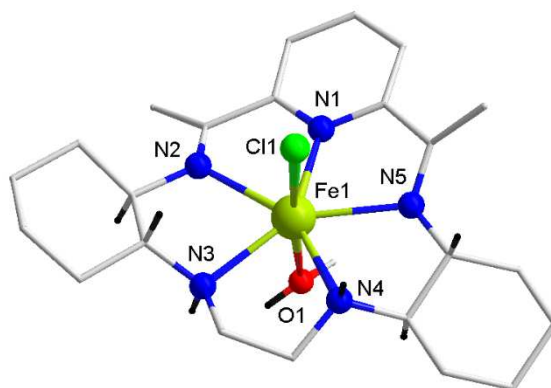


Figure 1. Molecular structure of complex $[\text{FeL}^{\text{N5R,R}}\text{Cl}(\text{MeOH})]^+$ in **1R**; some H atoms and the Cl^- counter anion are not depicted for clarity. H atoms in black and C in grey. Selected Fe1-Y bond distances (\AA): Y = N1, 2.173(1); N2, 2.282(1); N3, 2.305(1); N4, 2.262(1); N5, 2.345(1); Cl1, 2.4662(4); O1, 2.201(1) \AA .

The chain compounds $[\text{FeL}^{\text{N5R,R}}\{\text{FeCl}_4\}]$, **2R**, and $[\text{FeL}^{\text{N5S,S}}\{\text{FeCl}_4\}]$, **2S**, crystallized in tetragonal space group $P4_32_12$ and $P4_12_12$, respectively. They consist in an alternation of tetra- and hepta-coordinated Fe^{II} moieties made up by $[\text{FeL}^{\text{N5R,R}}]^{2+}$ or $[\text{FeL}^{\text{N5S,S}}]^{2+}$ and $[\text{FeCl}_4]^{2-}$ units linked by Cl atoms (Figure 2). Since they differ only by the chirality of the macrocyclic ligand (Figure S3), enantiomer **2R** is used for the forthcoming description. The coordination sphere of Fe1 accommodates the pentadentate ligand $\text{L}^{\text{N5R,R}}$ in the equatorial sites and two Cl atoms in the apical positions. The latter are each connected to a second metal center, Fe2, which displays a coordination sphere formed by four Cl atoms in approximately tetrahedral arrangement. Each $[\text{FeCl}_4]$ unit is also bound to two $[\text{FeL}^{\text{N5R,R}}]^{2+}$ centers, resulting in a straight 1D coordination polymer growing along the crystallographic c -direction. A comparison of the Fe-Cl bond lengths (see caption to the Figure 2) shows that the distance to Fe1 is sensibly longer than in **1R** and significantly longer than to Fe2. This supports the view that **2R** results from the assembly of $[\text{FeL}^{\text{N5R,R}}]^{2+}$ and $[\text{FeCl}_4]^{2-}$ units. The analyses by SHAPE of the coordination polyhedra of the metal centers confirmed a slightly distorted tetrahedral coordination sphere for Fe2 and a more distorted PBP geometry for Fe1 (Table S2) that may be related to the occupation disorder of the pentadentate ligand (*cf.* the Experimental Section).

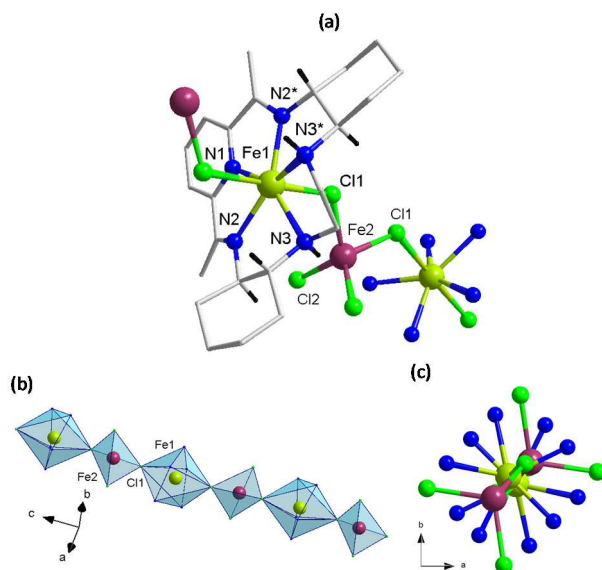


Figure 2. Crystal structure of $[\text{FeL}^{\text{NSR,R}}\{\text{FeCl}_4\}]$, **2R**. (a) arrangement of the molecular fragments, (b, c) simplified views of the chain structure (only 1st coordination spheres are shown). The PBP Fe1 are depicted in lime green and the Td Fe2 in plum red; * = 1-x,1-y,1.5-z. Selected bond lengths (Å): Fe1-Y with Y = Cl1, 2.5993(6); N1, 2.148(3); N2, 2.242(2); N3, 2.262(2); Fe2-Cl1, 2.3388(7); Fe2-Cl2, 2.2939(7).

Circular Dichroism

The optical activity of these complexes was confirmed by the circular dichroism (CD) spectra recorded for crystalline powders diluted in KBr (1 % in mass). The enantiomorphism of **1R** and **1S**, and **2R** and **2S** is confirmed by the spectra showing symmetrical signals but of opposite sign (Figure 3 for derivatives **2R/S** and Figure S4 for **1R/S**). The CD features can be assigned to d-d transitions (500-700 nm) and $\pi-\pi^*$ intra-ligand transitions (250-350 nm).

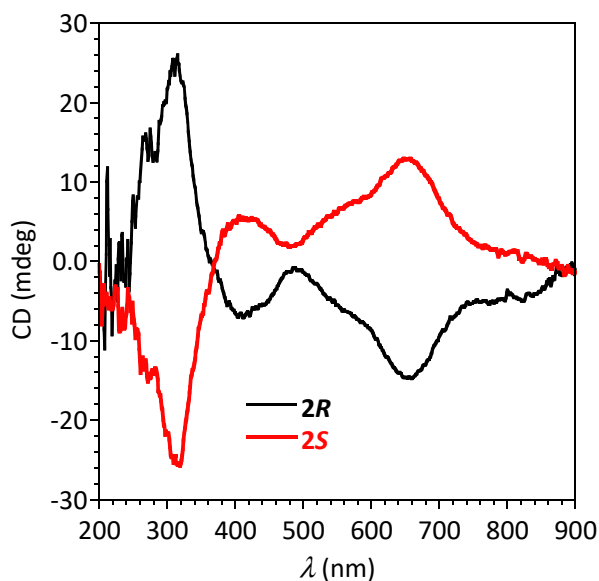


Figure 3. Solid state CD spectra for **2R** (in black) and **2S** (in red).

Magnetic properties.

The magnetic behaviors were studied for the *R* enantiomer of each derivative since the enantiomeric form does not affect the magnetic properties. The temperature dependence of the molar magnetic susceptibility, χ_M , for **1R** showed a paramagnetic behavior characterized by a $\chi_M T$ value $3.53 \text{ cm}^3 \text{ mol}^{-1} \text{ K}$ between 300 and 50 K (Figure 4), in agreement with the expected Curie constant for a $S = 2$ with a g slightly larger than 2. For lower T , a decrease in $\chi_M T$ was observed, reaching $2.33 \text{ cm}^3 \text{ mol}^{-1} \text{ K}$ at 2 K. The field dependence of the magnetization recorded between 2 and 8 K did not saturate even for largest applied field (i.e., 50 kOe). The low T behavior of $\chi_M T$ and the magnetizations suggested the effect of magnetic anisotropy, as is expected for Fe^{II} in PBP coordination sphere.¹⁶ This anisotropy was evaluated by considering a zero-field splitting (ZFS) effect and led to axial parameter $D = -5.9 \pm 0.1 \text{ cm}^{-1}$ and $g = 2.169 \pm 0.002$ by a simultaneous analysis of the $\chi_M T = f(T)$ and $M = f(H)$ behaviors using the PHI software.³⁰ The value found for D is in accordance with those reported for related Fe^{II} complexes displaying O-ligands in the apical coordination positions,³¹ and confirmed an easy-axis magnetic anisotropy. AC magnetic susceptibility did not exhibit an out-of-phase component, χ_M'' , whether realized in the absence or in an applied static magnetic field.

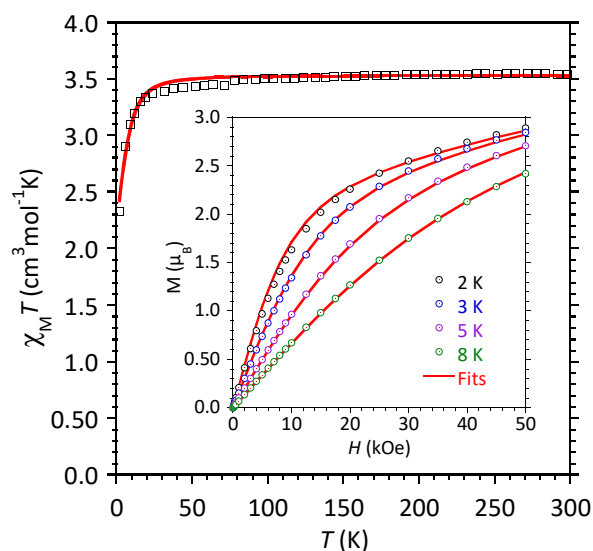


Figure 4. $\chi_M T = f(T)$ and (insert) $M = f(H)$ behaviors for $[\text{FeL}^{\text{N5R,R}}\text{Cl}(\text{MeOH})]\text{Cl}$, **1R**; the red lines are the best fits.

For $[\text{FeL}^{\text{N5R,R}}\{\text{FeCl}_4\}]$, **2R**, the $\chi_M T = f(T)$ behavior was characteristic for antiferromagnetic interactions between the Fe centers (Figure 5). At 300 K the value for $\chi_M T$ was $6.25 \text{ cm}^3 \text{ mol}^{-1} \text{ K}$, in agreement with the anticipated contributions of two $S = 2$ spin centers, and steadily decreased as T was lowered. However, instead of reaching a non-magnetic ground state, a plateau with about $1.70 \text{ cm}^3 \text{ mol}^{-1} \text{ K}$ was observed between 15 and 4 K (black plot in Figure 5), before $\chi_M T$ decreased again to reach $1.17 \text{ cm}^3 \text{ mol}^{-1} \text{ K}$ for 2 K. When the applied field was reduced from 1 kOe to 25 Oe, instead of remaining constant below 15 K, $\chi_M T$ exhibited a rise with sharp increase (blue plot in Figure 5), reaching $6.18 \text{ cm}^3 \text{ mol}^{-1} \text{ K}$ for 3.5 K. For an even smaller applied field of 10 Oe, the same rise was observed but the maximum value reached was $3.87 \text{ cm}^3 \text{ mol}^{-1} \text{ K}$ for 3.5 K. The field dependence of the magnetization recorded between 2 and 8 K showed a steady increase (linear slope above 1.5 Tesla, see Figure S5) with field to reach $1.2 \mu_B$ for 5 Tesla. Such behaviors revealed that below 6 K the local magnetic moments do not compensate each other resulting in the growth of a small magnetization for the 1-D organizations

(insert Figure 5 and Figure S5a), a feature that is cancelled for larger fields due to the gradual alignment of the spins with field. This is characteristic for canted antiferromagnetic interactions, also known as weak ferromagnetism.

The exchange interaction between the Fe centers was assessed by analyzing the behavior of $\chi_M T$ with an expression of the susceptibility for an Heisenberg linear chain with alternating spins ($H = -J_{i,j} \sum_{(i,j)} \mathbf{S}_i \cdot \mathbf{S}_j$).^{32, 33} A perfect fit was obtained between 300 and 12 K considering two spins of $S = 2$ with different g , resulting in $J_{\text{FeFe}} = -6.14 \pm 0.05 \text{ cm}^{-1}$, $g_1 = 1.911 \pm 0.004$, $g_2 = 2.397 \pm 0.003$. The susceptibility data are also well reproduced between 300 and 17 K by a single-center chain model³⁴ ($H = -J \sum_{i=n}^{n-1} S_{A_i} \cdot S_{A_{i+1}}$) leading to $J_{\text{FeFe}} = -5.63 \pm 0.05 \text{ cm}^{-1}$ and $g = 2.157 \pm 0.003$ (Figure S5). The obtained values are consistent with reported Cl-mediated exchange interactions.^{35, 36}

From the magnetization at 2 K a spin canting angle of $\alpha = 2.6^\circ$ was deduced using $\sin \alpha = M_W/M_S$,³⁴ where M_W is the initial magnetization ($0.40 \mu_B$, see Figure S5d) and M_S the saturation magnetization calculated using the mean g factor deduced from the above analysis of $\chi_M T$ versus T .

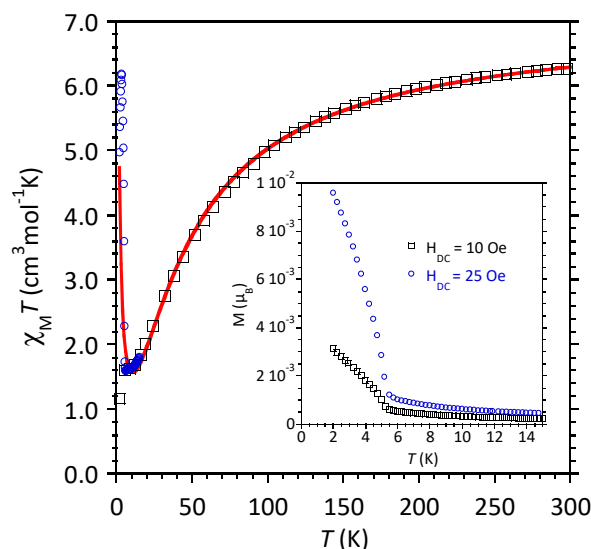


Figure 5. $\chi_M T = f(T)$ behavior for $[\text{FeL}^{\text{N5R,R}}\{\text{FeCl}_4\}]$, **2R**: experimental behavior with $H = 25$ (in blue) and 1000 Oe (in black) and best fit (in red) of a ferrimagnetic chain model for two $S = 2$ with different g (see text). Insert: FCM with applied field of 10 and 25 Oe; see also Figure S5.

The temperature and frequency dependencies of the AC magnetic susceptibility for **2R**, obtained in absence of a static magnetic field, were characteristic for slow relaxation of the magnetization. The out-of-phase susceptibility, χ_M'' , as a function of temperature was found frequency dependent (Figure 6a) as was the χ_M'' versus ν behavior as a function of T (Figure S6). An anomaly can be noticed in temperature dependence of χ_M' and χ_M'' in the form of a slight peak at 5.2 K that is independent of the frequency. This temperature corresponds also to the step in the FC and ZFC magnetizations and to the vanishing of the remanant magnetization (Figure S5a). It must be concluded that a canted antiferromagnetic ordering occurs with the emergence of SCM behavior for 1D $[\text{FeL}^{\text{N5R,R}}\{\text{FeCl}_4\}]$. Slow relaxation of the magnetization for 1-D spin arrays at temperatures below a magnetic ordering is not uncommon.³⁷⁻⁴³

The relaxation time, τ , between 2 and 3 K could be assessed by the analysis of χ_M'' versus ν with an extended Debye model, its temperature dependence is plotted in Figure 6b. The linear variation of $\ln \tau$

versus $1/T$ was well reproduced by the Arrhenius equation to give an energy barrier for magnetization flipping of $\Delta/k_B = 42$ K with pre-exponential factor, $\tau_0 = 2.17 \times 10^{-10}$ s. In the present system, the contribution of the exchange correlation to the energy barrier cannot be assessed as usually done for ferro- or ferrimagnetic SCM (see Figure S5f).

These characteristics are in agreement with a SCM behavior for **2R**. While scarce, SCM behaviors for homometallic canted antiferromagnetic chains involving PBP Fe^{II} centers were reported.^{19, 20, 22} It is interesting to note that the energy barrier Δ/k_B in **2R** is slightly larger than that found for cyanide-bridged derivatives^{19, 20} but significantly smaller than for an azido-bridged chain (87 K).²² For the compounds described earlier, the activation barriers can be related to the relative orientations of the axes of easy magnetizations of the PBP centers, but this is less evident in **2R** due to the alternating tetra-coordinated and PBP Fe^{II} units. Theoretical studies have been undertaken to clarify this situation.

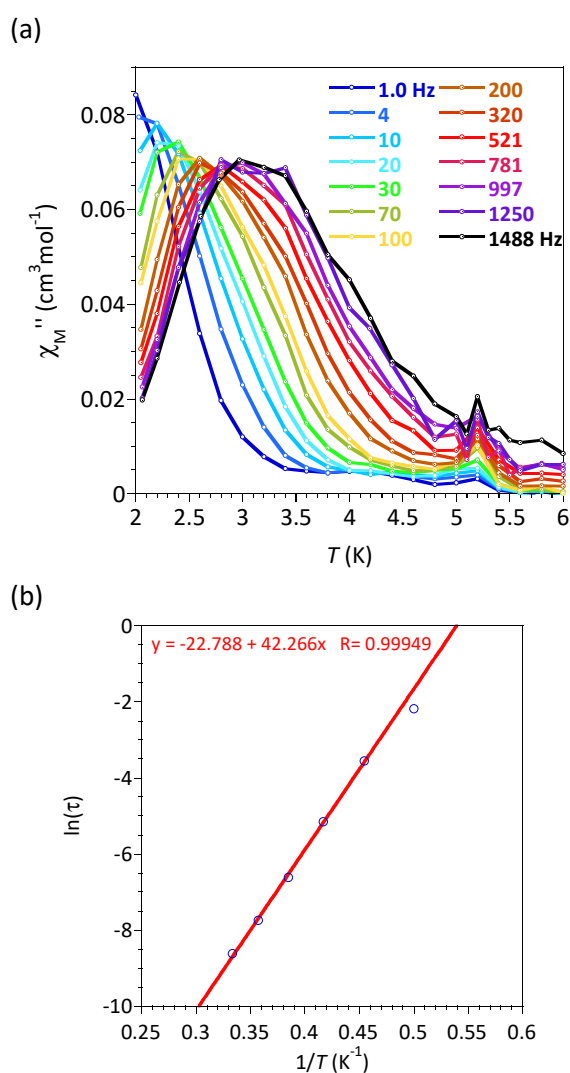


Figure 6. AC magnetic susceptibility for **2R** : (a) χ_M'' versus T and (b) $\ln(\tau) = 1/T$ with best fit to the Arrhenius equation (red full line).

Theoretical calculations

In order to determine the magnetic coupling between nearest-neighbor Fe^{II} centers, two different fragments of the chain were considered. The first one, F1, is centered on a [FeCl₄]²⁻ moiety linked to two [FeL^{N5R,R}]²⁺ moieties which are themselves bordered by a [ZnCl₄]²⁻ (located on each side of the fragment) as depicted on Figure S7a. The Zn^{II} being closed shell, they do not contribute to the magnetism of the calculated complex. The second fragment F2 is built according to the same logic but centered on the [FeL^{N5R,R}]²⁺ moiety (Figure S7b). Let us consider the Ising model $\hat{H}^{Ising} = -J\hat{S}_{Z_1}\hat{S}_{Z_2} - J\hat{S}_{Z_2}\hat{S}_{Z_3}$ defined on the three magnetic ions numbered from left to right and where J is the magnetic coupling and \hat{S}_{Z_1} , \hat{S}_{Z_2} and \hat{S}_{Z_3} are the spin operator projection on z for the centers 1, 2, and 3, respectively. Three different broken spin symmetry DFT solutions have been calculated for the two fragments:

- i) the first solution with $M_s = 6$ contains three $m_s = 2$ local solutions (one on each Fe^{II}) and is noted $\uparrow\uparrow\uparrow$: its Ising energy is $-8J$,
- ii) the second solution has $M_s = 2$ and contains two $m_s = 2$ local solutions (on centers 1 and 3) and one $m_s = -2$ local solution (on center 2) and is noted $\uparrow\downarrow\uparrow$; its energy is $8J$,
- iii) the third one has also $M_s = 2$ and two $m_s = 2$ local solutions but on centers 1 and 2, and one $m_s = -2$ local solution on center 3. It is noted $\uparrow\uparrow\downarrow$ and its energy is zero.

The different values of the antiferromagnetic couplings extracted from the energy differences between the various solutions and for the two fragments are reported in Table 1. They are very consistent ($J \sim -8 \text{ cm}^{-1}$) showing that the consideration of different fragments of the chain, or different DFT solutions, does not introduce any bias for the evaluation of the magnetic coupling.

Fragment	Solutions used	$\Delta E \text{ (cm}^{-1}\text{)}$	$J \text{ (cm}^{-1}\text{)}$
F1	$\uparrow\uparrow\uparrow$ and $\uparrow\downarrow\uparrow$	$16J = -129$	-8.1
	$\uparrow\uparrow\uparrow$ and $\uparrow\uparrow\downarrow$	$8J = -68$	-8.5
F2	$\uparrow\uparrow\uparrow$ and $\uparrow\downarrow\uparrow$	$16J = -125$	-7.8
	$\uparrow\uparrow\uparrow$ and $\uparrow\uparrow\downarrow$	$8J = -64$	-8.0

Table 1. Energy differences between the different DFT M_s solutions (see text) and nearest-neighbor magnetic coupling in cm^{-1} obtained for the two different fragments considered.

The method used to evaluate the magnetic anisotropy parameters of the two Fe^{II} centers has been extensively described before and successfully applied to many transition metal complexes;⁴⁴ its main features are recalled in the Computational Information section. *Ab initio* calculations were carried out on two fragments F1' and F2' respectively related to F1 and F2 (Figure S7) but now only the central Fe^{II} was kept and all surrounding metal ions have been substituted by Zn^{II} ions, *i.e.* there is a single magnetic ion explicitly considered in the calculation.

The value of the D and E parameters and the contributions of the most involved excited states are given in Table 2. A perturbative evaluation of these contributions is easily accessed by applying the following simplified spin-orbit coupling (SOC) operator: $\zeta \sum_i (l_i^Z s_i^Z + (l_i^+ s_i^- + l_i^- s_i^+)/2)$ where ζ is the spin-orbit coupling constant of the free ion. We recall that if the excited state and ground state are of the same spin and are coupled by the $l_z s_z$ part of the SOC operator, the contribution is negative while

it is positive if they are coupled through $(l^+s^- + l^-s^+)/2$. The d_{xy} and $d_{x^2-y^2}$ orbitals are linear combinations of the d_{2-} and d_{2+} spherical harmonics, d_{xz} and d_{yz} are linear combinations of the d_{1-} to the d_{1+} and $d_{z^2} = d_0$.

For $[\text{FeCl}_4]^{2-}$ an axial ZFS parameter $D = 15.10 \text{ cm}^{-1}$ and a rhombic parameter $E = 3.6 \text{ cm}^{-1}$ ($E/D = 0.24$) were obtained. This unit has a highly distorted tetrahedral geometry, so that the MO diagram (Figure 7) shows large lifts of degeneracy of the lowest d_{z^2} and $d_{x^2-y^2}$ and highest d_{yz} , d_{xz} and d_{xy} orbitals. The doubly occupied orbital in the ground state wave function is the d_{z^2} orbital, so interactions through SOC can only couple the ground state with the first, second and third excited quintet states in which some determinants have either a d_{yz} or d_{xz} doubly occupied orbital. These couplings through the $(l^+s^- + l^-s^+)/2$ operator generate important positive contributions to the overall D and rationalize both the nature and magnitude of this axial parameter. The magnetic axes are pictured in Figure 8 and Figure S8.

For the PBP Fe center, the MO diagram (Figure 7) displays nearly degenerate orbital pairs (d_{yz} and d_{xz}) and ($d_{x^2-y^2}$ and d_{xy}). For this reason, the ground state is almost degenerate with the first excited one, the two electrons occupying either the d_{xz} or the d_{yz} orbital. As a result, a first order SOC is obtained and the coupling through the $l_z s_z$ part of the spin-orbit operator generates a strong negative D contribution. The other excited quintets and some excited triplets provide a small positive contribution (Table 2), finally resulting to the axial parameter $D = -28.6 \text{ cm}^{-1}$ and $E = 0.3 \text{ cm}^{-1}$ ($E/D = 0.01$). The easy magnetic axis of this Fe^{II} center is aligned along the apical coordination sites (blue arrow in Figure 8), in agreement with earlier reports on PBP Fe^{II} complexes.^{21, 31, 45-47}

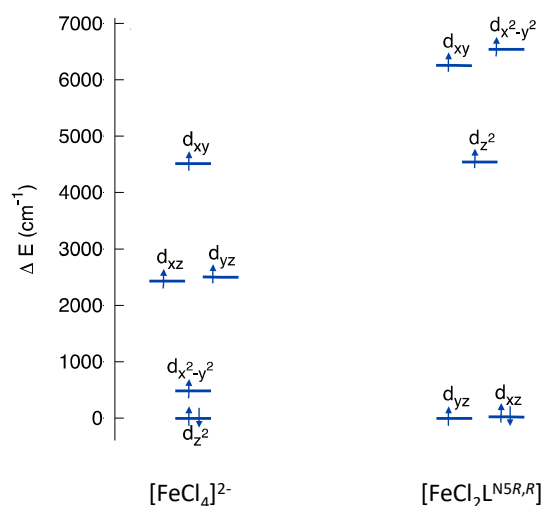


Figure 7. Molecular orbital diagrams for the $[\text{FeCl}_4]^{2-}$ (left) and $[\text{FeCl}_2\text{L}^{\text{N5R,R}}]$ (right) moieties obtained by ab initio ligand field theory (AILFT) calculations.

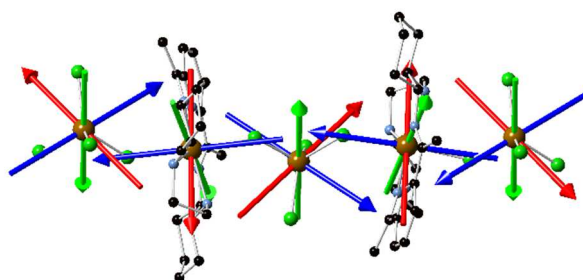


Figure 8. Calculated magnetic axes (x in red, y in green, and z in blue) for the Fe^{II} centers in 1-D [FeL^{NSR,R}][FeCl₄], **2R**.

Unit	States	State energies	Determinants	Contribution to <i>D</i>	Contribution to <i>E</i>
[FeCl₄] in F1'					
	Q ₀	0	<i>d_{z²}</i> : 99%	-	-
	Q ₁	475	<i>d_{x²-y²}</i> : 76% <i>d_{xz}</i> : 24%	5.15	5.15
	Q ₂	2865	<i>d_{x²-y²}</i> : 23% <i>d_{xz}</i> : 76%	3.93	3.93
	Q ₃	2946	<i>d_{yz}</i> : 100%	5.25	-5.28
	Q ₄	5290	<i>d_{xy}</i> : 100%	-0.02	0.00
				<i>D</i> = 15.0 cm ⁻¹ [a]	<i>E/D</i> =0.24
[FeCl₂L^{NSR,R}] in F2'					
	Q ₀	0	<i>d_{xz}</i> : 96%	-	-
	Q ₁	66	<i>d_{yz}</i> : 98%	-34.4	0.01
	Q ₂	6180	<i>d_{z²}</i> : 96%	1.80	1.74
	Q ₃	7860	<i>d_{xy}</i> : 96%	0.64	-0.59
	Q ₄	8120	<i>d_{x²-y²}</i> : 94%	0.77	1.00
				<i>D</i> =-28.6 cm ⁻¹ [b]	<i>E/D</i> =0.01

[a] for [FeCl₄], $g_x = 1.977374$, $g_y = 2.178993$, $g_z = 2.324633$, $D_{xx} = 3.907399$, $D_{yy} = -3.179984$, and $D_{zz} = 15.349959$. [b] for [FeCl₂L^{NSR,R}] $g_x = 1.831767$, $g_y = 1.887831$, $g_z = 2.539879$, $D_{xx} = 9.333804$, $D_{yy} = 9.729339$, and $D_{zz} = -19.063143$.

Table 2. NEVPT2 energies, main determinants and their weight in the CASSCF wave functions, second order perturbation evaluation from NEVPT2 results of the main contributions to *D* and *E* of all the quintet excited states. All values are given in cm⁻¹. Only the doubly occupied orbital of the determinant is indicated.

It was gratifying to find good agreement between the calculated and experimental values. In both cases an antiferromagnetic exchange interaction was obtained, respectively in the order of -8 cm⁻¹ and -6.1 cm⁻¹. Regarding the anisotropy parameters, the stronger axuality obtained for the PBP Fe^{II} in the chain as compared to **1R** is coherent with earlier results that revealed a smaller energy difference for the *d_{xz}* and *d_{yz}* orbital for Cl than for O-atoms in the apical positions, hence more negative *D* values for the former complexes.^{17, 31} The rather long bonds between Cl to Fe^{II} in **2R**, contribute to stabilize these orbitals and further reduce their energy difference, which explains the strongly negative *D* obtained for the PBP units in [FeL^{NSR,R}][FeCl₄]. A positive *D* was obtained for the [FeCl₄] unit, leading to the description of **2R** as a 1D spin lattice consisting of an alternation of centers with axial and planar magnetic anisotropy.

The calculated magnetic axis for the respective Fe^{II} centers were affixed to the chain [FeL^{N5R,R}{FeCl₄}] in Figure 8. As a result of the antiferromagnetic interactions, the moments located on the PBP centers point in the same direction but they are clearly not parallel; an angle of 31° is found between the easy-axis (blue arrows) of the PBP Fe^{II} units. The interplay between nearest neighbor local magnetic anisotropies, and hence the resulting overall magnetic anisotropy, is more difficult to evaluate because it depends on their relative orientations.⁴⁸ However, based on model systems,⁴⁸ the situation arising in **2R** should result in an overall axial anisotropy which is supported by the SCM behavior exhibited by the compound.

CONCLUDING REMARKS

The originality of the homochiral SCM obtained by using a chlorine atom as bridging ligand between Fe^{II} centers is multiple.

It is the first example of SCM constructed from PBP Fe^{II} centers in association with a complementary unit bearing also substantial magnetic anisotropy. The resulting spin array consists in high-spin Fe^{II} of alternating easy-axis and easy-plane anisotropy with $D = -28.6$ and 15 cm^{-1} , respectively.

The magnetic anisotropy for the PBP center is the largest reported so far for Fe^{II} in this coordination polyhedron, a characteristic that can be attributed to the rather long bond lengths with the Cl ligands in the axial positions. Indeed, such a feature leads to a large energy difference between the two low-lying orbitals (d_{xz} and d_{yz}) and the other orbitals, and thus D results mainly from the large negative contribution of the first excited state, the positive contributions from the other excited states being drastically reduced.

For this homo-spin system, the observation of slow relaxation of the magnetization not only revealed an overall axial anisotropy but mainly a canted antiferromagnetic behavior. It should be noted that the SCM behavior is found in the ordered phase where the compound behaves as a weak ferromagnet, *i.e.* a canted antiferromagnet. Noteworthy, the energy barrier of the thermally activated magnetization flipping for **2R** ($\Delta/k_B = 42 \text{ K}$) is in the range of that found for other SCMs involving PBP Fe^{II} centers as Ising-type anisotropy units.

Finally, the novel chiral Fe^{II} complex involved as building block of the chain compound appears ideally suited to implement controlled chirality and magnetic anisotropy in a polynuclear derivative. Both enantiomers are readily accessible by the means of the enantiopure macrocyclic pentadentate ligand.

EXPERIMENTAL SECTION

Materials and methods: All reagents and solvents were used as received from commercial sources unless otherwise specified. Dichloromethane (DCM) and tetrahydrofuran (THF) were purified using an *Innovative Technology Solvent Purification*[®] system under an argon atmosphere. Methanol was dried over Mg(OMe)₂, distilled under nitrogen and stored on activated molecular sieves (4 Å) in a glovebox. The syntheses involving Fe^{II} salts were performed in glovebox operating under argon atmosphere. The preparation of N,N'-Bis{(1*R*,2*R*)-[2-(amino)]cyclohexyl}-1,2-diaminoethane tetrachlorhydrate and its *S*-enantiomer can be found in the SI. The solid samples for the characterizations were prepared in a glovebox. Fourier transform infrared (FT-IR) spectroscopy was performed with a Perkin–Elmer spectrum GX 2000 FT-IR spectrometer. UV-Visible absorption and circular dichroism (CD) spectroscopic measurements were performed on a Jasco J-815 spectropolarimeter at room temperature between 200 and 900 nm with 2 nm pitch and bandwidth, 10 nm/min scan speed. Spectra were recorded on pellets of freshly isolated crystalline powders diluted in KBr (1 %mass). Elemental analyses were

performed with a Perkin–Elmer 2400 series II instrument. Magnetic studies were carried out with a Quantum Design MPMS-5S SQUID magnetometer on freshly isolated polycrystalline powders mixed with eicosane and held in quartz tubes. Data have been collected between 300 and 2 K with an applied field of 1 kOe and corrected for the diamagnetic contribution sample by using Pascal's tables³⁴ and for the sample holder. The field dependences of the magnetization were measured between 2 and 8 K with dc magnetic field up to 5 T. The absence of ferromagnetic impurities was checked by measurement of M vs. H at 100 K. AC magnetic susceptibility data were recorded with $H_{AC} = 3$ Oe in the frequency range 1 to 1500 Hz. Powder X-Ray diffraction (PXRD) patterns were recorded in transmission mode using capillary tubes on a XPert Pro (Theta–Theta mode) Panalytical diffractometer with $\lambda(\text{Cu}_{K\alpha 1, K\alpha 2}) = 1.54059$ and 1.54439 Å.

Synthesis: R and S enantiomers of each compound were obtained by same procedure, therefore only that for **1R** and **2R** are described.

[Fe(L^{N5R,R})Cl(MeOH)]Cl·H₂O, 1R: FeCl₂·4H₂O (199 mg, 1 mmol) in 10 mL MeOH was added to a methanolic solution of diacetylpyridine (162 mg, 1 mmol, 10 mL). The violet solution was refluxed 1 h and darkened with time. Meanwhile, N,N'-Bis{(1R,2R)-[2-(amino)cyclohexyl]-1,2-diaminoethane tetrachlorhydrate (400 mg, 1 mmol) was suspended in 20 mL MeOH and ^tBuOK (448 mg, 4 mmol) dissolved in 15 mL MeOH was added. The suspension was stirred at room temperature for 30 minutes before the solution was added to the violet solution containing the Fe derivative. A color change to dark blue took place rapidly. The mixture was refluxed during 3 days to complete the reaction (after about 12 h, the medium is clear with no suspension). The dark blue solution was evaporated under vacuum and the residue suspended in 4 mL of CH₂Cl₂. The resulting suspension was stirred 1 night at room temperature before filtration on frit (to discard KCl salts). The solid was further washed with CH₂Cl₂ (about 1 mL) until complete fading. About 10 mL of Et₂O were added drop by drop to the blue solution till apparition of a solid and the flask was stored at 4°C. After 3 days a first batch of **1R** was collected as polycrystalline dark blue solid (420 mg). The blue filtrate was further concentrated to approximately 1-2 mL (till solid formation on the walls) and 6 mL Et₂O was layered on top. Additional crystalline blue solid (30 mg) was isolated after 2 days. The total amount of **1R** collected was 450 mg (Yield: 84 %). Polycrystalline solid with mother solution in a capillary gave a powder diffraction pattern in agreement with the one calculated for **1R** (Figure S1a). IR (ATR Ge, cm⁻¹): 3357 (br), 3278 (m), 3262 (m), 3237 (br), 3198 (br), 2962 (m), 2935 (m), 2863 (m), 1700 (w), 1642 (m), 1592 (w), 1447 (m), 1371 (sh), 1260 (m), 1199 (w), 1089 (m), 1019 (m), 960 (w), 940 (w), 901 (w), 867 (w), 788 (s), 702 (w), 684 (w), 663 (w), 639 (w), 623 (m). Elemental analysis (%) calcd. for C₂₄H₄₁Cl₂FeN₅O₂ ([Fe(L^{N5R,R})(MeOH)Cl]Cl·H₂O): C 51.63; H 7.40; N 12.54; found: C 51.66; H 7.00; N 12.43. For **1S**: Yield: 450 mg (87 %). Phase purity of the polycrystalline solid was confirmed by PXRD (Figure S1b). Elemental analysis (%) calcd. for C₂₄H₄₁Cl₂FeN₅O₂ ([Fe(L^{N5S,S})(MeOH)Cl]Cl·H₂O): C 51.63; H 7.40; N 12.54; found: C 51.26; H 7.20; N 12.33.

[Fe(L^{N5R,R})FeCl₄], 2R: FeCl₂·4H₂O (148 mg, 0.74 mmol) and [Fe(L^{N5R,R})Cl(MeOH)]Cl·H₂O (400 mg, 0.74 mmol) were dissolved in 25 mL MeOH and the resulting dark blue solution was refluxed 1 day. After cooling to room temperature, the mixture was evaporated to dryness. The solid was dispersed in 7 mL of CH₂Cl₂ mixed with 0.2 mL MeOH and the suspension was stirred 1 day before filtration (PTFE filter 0.45 mm). Diethyl ether (10 mL) was layered on top of the filtrate. After inter-diffusion, **2R** was isolated as deep blue crystals (350 mg, yield: 77 %). IR (ATR Ge, cm⁻¹): 3391 (br), 3221 (w), 3191 (m), 3044 (w), 2937 (m), 2963 (w), 2858 (w), 1645 (m), 1593 (m), 1445 (m), 1426 (sh), 1406 (m), 1369 (m), 1326 (w), 1300 (w), 1261 (m), 1243 (w), 1220 (w), 1196 (m), 1143 (w), 1133 (m), 1094 (w), 1053 (sh), 1021 (m),

968 (m), 905 (sh), 839 (s), 815 (s), 749 (w), 737 (w), 684 (w), 664 (w), 650 (w). Elemental analysis (%) calcd. for $C_{23}H_{35}Cl_4Fe_2N_5$ ($[Fe(L^{N5R,R})FeCl_4]$): C 43.50; H 5.56; N 11.03; found: C 43.17; H 5.83; N 10.73. **2S**: Elemental analysis (%) calcd. for $C_{23}H_{35}Cl_4Fe_2N_5$ ($[Fe(L^{N5S,S})FeCl_4]$): C 43.50; H 5.56; N 11.03; found: C 43.30; H 5.71; N 11.3. Phase purity of the polycrystalline solid was confirmed by PXRD (Figure S1d).

Single-crystal X-ray diffraction:

Single crystals suitable for X-ray diffraction were coated with paratone oil and mounted onto the goniometer. The X-ray crystallographic data were obtained at 100K on a Rigaku XtaLAB Synergy or a Bruker Apex2 diffractometer equipped with an Oxford Cryosystem. The structures have been solved using ShelXT or Superflip and refined by means of least-squares procedures on F or F^2 using the program CRYSTALS.⁴⁹ The scattering factors for all the atoms were used as listed in the International Tables for X-ray Crystallography.⁵⁰ Absorption correction was performed using a multiscan procedure. All non-hydrogen atoms were refined anisotropically. The H atoms were refined with riding constraints. The structures for **2R** and **2S** presented treated statistic disorders on the cyclohexyl moieties. Refinement of the final formulated models leads to imperfect but reasonable solutions. Crystallographic information for all the complexes are gathered in Table S1. The crystallographic information (cif) for the structures has been deposited at CCDC (www.ccdc.cam.ac.uk/data_request/cif) under deposition number(s) 2214580-2214583.

Computational Information:

Theoretical calculations have been performed with the ORCA(5.0) code.^{51, 52} X-Ray geometries were considered in all calculations, except for the hydrogens positions that have been optimized by Density Functional Theory (DFT) calculations using the PBE functional⁵³ and def2-SVP basis sets (5s3p2d1f for Fe and Zn, 4s3p1d for Cl, 3s2p1d for C and N, and 2s1p for H).⁵⁴

DFT calculations of the magnetic couplings have been performed using the wb97X-D3 functional,⁵⁵ which usually provides accurate values of magnetic couplings,⁵⁶ and the following basis atomic sets: def2-TZVP for the Fe centers and their first coordination sphere atoms (6s4p4d1f for Fe, 5s5p2d1f for Cl and 5s3p2d1f for N) and def2-SVP for remote atoms (5s3p2d1f for Zn, 4s3p1d for Cl, 3s2p1d for C and N and 2s1p for H).

The *ab initio* method used here to determine the magnetic anisotropy parameters has been successfully applied to many transition metal complexes.⁴⁴ It consists in a two-step procedure: i) in a first place, spin-orbit free electronic states are calculated using the Complete Active Space State Self Consistent Field (CASSCF) method. The active space considered all d electrons in all d-orbitals of the metal ions, *i.e.* CAS(6,5), and all the orbitals are optimized in a state average way on all the states of the configuration, *i.e.* 10 quintets, 45 triplets and 50 singlets. Dynamic correlations are treated perturbatively using the n-electron valence state perturbation theory (NEVPT2) method.⁵⁷ ii) In the second step, relativistic effects are introduced using the spin-orbit state interaction SO-SI method which couples all Ms components of the spin-orbit free states calculated previously.⁵⁸ The extraction of the anisotropy parameters uses the effective Hamiltonian theory which permits the numerical determination of all ZFS tensor elements.^{59, 60} The following basis sets have been used: DKH-def2 for Fe^{II} , the atoms of its first coordination sphere, and the two closest Zn^{II} (*i.e.* 6s4p4d1f for Fe, 6s5p4d1f for Zn, 5s5p2d1f for Cl and 5s3p2d1f for N) and DKH-def2-SVP for the other atoms (9s5p2d1f for the two other Zn^{II} , 6s3p1d for the other Cl, 3s2p1d for C, and 2s1p for H).⁵⁴

SUPPORTING INFORMATION

Experimental procedures; crystallographic and geometric information; polyhedral shape analyses of the coordination spheres; additional magnetic data, and results from the calculations. The crystallographic information for the structures has been deposited at CCDC under numbers: CCDC-2214580 (for **1S**), CCDC-2214581 (for **1R**), CCDC-2214582 (for **2S**), CCDC-22145808 (for **2R**), these cifs contain(s) the supplementary crystallographic data for this paper and are provided free of charge by the joint Cambridge Crystallographic Data Centre and Fachinformationszentrum Karlsruhe via <http://www.ccdc.cam.ac.uk/structures>

ACKNOWLEDGEMENT

This work was supported by the French National Research Agency, ANR, (grant ANR-17-CE07-0007). Authors are grateful to M. J.-F. Meunier (LCC) and Charles-Louis Serpentine (IMRCP, Université de Toulouse) for technical assistance in magnetic data collections and circular dichroic measurements.

REFERENCES

- (1) Gatteschi, D.; Sessoli, R.; Villain, J. *Molecular Nanomagnets*; Oxford University Press, 2006.
- (2) Coulon, C.; Miyasaka, H.; Clérac, R. Single-chain magnets: Theoretical approach and experimental systems. In *Single-Molecule Magnets and Related Phenomena*, Winpenny, R. Ed.; Structure and Bonding, Vol. 122; Springer, 2006; pp 163-206. DOI: <https://doi.org/10.1007/b104234>
- (3) Coulon, C.; Pianet, V.; Urdampilleta, M.; Clérac, R. Single-Chain Magnets and Related Systems. In *Molecular Nanomagnets and Related Phenomena*, Gao, S. Ed.; Structure and Bonding, Vol. 164; Springer Berlin Heidelberg, 2015; pp 143-184. DOI: 10.1007/430_2014_154
- (4) Bogani, L.; Vindigni, A.; Sessoli, R.; Gatteschi, D. Single chain magnets: where to from here ? *J. Mater. Chem.* **2008**, *18*, 4750-4758. DOI : <https://doi.org/10.1039/B807824F>
- (5) Atzori, M.; Rikken, G. L. J. A.; Train, C. Magneto-Chiral Dichroism: A Playground for Molecular Chemists. *Chem. Eur. J.* **2020**, *26*, 9784-9791. DOI: 10.1002/chem.202000937.
- (6) Train, C.; Gheorghe, R.; Krstic, V.; Chamoreau, L.-M.; Ovanesyan, N.; Rikken, G. L. J. A.; Gruselle, M.; Verdaguer, M. Strong magneto-chiral dichroism in enantiopure chiral ferromagnets. *Nat. Mater* **2008**, *7*, 729-734. DOI: <https://doi.org/10.1038/nmat2256>
- (7) Sessoli, R.; Boulon, M.-E.; Caneschi, A.; Mannini, M.; Poggini, L.; Wilhelm, F.; Rogalev, A. Strong magneto-chiral dichroism in a paramagnetic molecular helix observed by hard X-rays. *Nat Phys* **2015**, *11* (1), 69-74. DOI: 10.1038/nphys3152.
- (8) Atzori, M.; Breslavetz, I.; Paillet, K.; Inoue, K.; Rikken, G. L. J. A.; Train, C. A Chiral Prussian Blue Analogue Pushes Magneto-Chiral Dichroism Limits. *J. Am. Chem. Soc.* **2019**, *141* (51), 20022-20025. DOI: 10.1021/jacs.9b10970.
- (9) Taniguchi, K.; Nishio, M.; Kishiue, S.; Huang, P.-J.; Kimura, S.; Miyasaka, H. Strong magnetochiral dichroism for visible light emission in a rationally designed paramagnetic enantiopure molecule. *Phys. Rev. Mater.* **2019**, *3* (4), 045202. DOI: 10.1103/PhysRevMaterials.3.045202.
- (10) Liu, C.-M.; Sun, R.; Wang, B.-W.; Wu, F.; Hao, X.; Shen, Z. Homochiral Ferromagnetic Coupling Dy₂ Single-Molecule Magnets with Strong Magneto-Optical Faraday Effects at Room Temperature. *Inorg. Chem.* **2021**, *60* (16), 12039-12048. DOI: 10.1021/acs.inorgchem.1c01218.
- (11) Riehl, J. P.; Richardson, F. S. Circularly polarized luminescence spectroscopy. *Chem. Rev.* **1986**, *86* (1), 1-16. DOI: 10.1021/cr00071a001.
- (12) Müller, K.; Fuchs, F.; Kneubühl, F. K. Partial circular polarization of the spectral thermal emission from ferromagnetic iron. *Phys. Lett. A* **1977**, *64* (2), 249-250. DOI: [https://doi.org/10.1016/0375-9601\(77\)90732-0](https://doi.org/10.1016/0375-9601(77)90732-0).
- (13) Elrez, B.; Liu, J.; Béreau, V.; Duhayon, C.; Horino, Y.; Suzuki, T.; Coolen, L.; Sutter, J.-P. Concomitant emergence of circularly polarized luminescence and single-molecule magnet behavior in chiral-at-metal Dy complex. *Inorg. Chem. Front.* **2020**, *7* (22), 4527-4534. DOI: 10.1039/D0QI00919A.
- (14) Pedersen, K. S.; Bendix, J.; Clerac, R. Single-molecule magnet engineering: building-block approaches. *Chem. Comm.* **2014**, *50* (34), 4396-4415. DOI: 10.1039/C4CC00339J.
- (15) Dhers, S.; Feltham, H. L. C.; Brooker, S. A toolbox of building blocks, linkers and crystallisation methods used to generate single-chain magnets. *Coord. Chem. Rev.* **2015**, *296*, 24-44. DOI: <https://doi.org/10.1016/j.ccr.2015.03.012>.
- (16) Sutter, J.-P.; Béreau, V.; Jubault, V.; Bretosh, K.; Pichon, C.; Duhayon, C. Magnetic anisotropy of transition metal and lanthanide ions in pentagonal bipyramidal geometry. *Chem. Soc. Rev.* **2022**, *51*, 3280-3313. DOI: 10.1039/D2CS00028H.
- (17) Bar, A. K.; Pichon, C.; Gogoi, N.; Duhayon, C.; Ramasesha, S.; Sutter, J.-P. Single-ion magnet behaviour of heptacoordinated Fe(II) complexes: on the importance of supramolecular organization. *Chem. Comm.* **2015**, *51* (17), 3616-3619. DOI: 10.1039/C4CC10182K.

- (18) Venkatakrisnan, T. S.; Sahoo, S.; Bréfuel, N.; Duhayon, C.; Paulsen, C.; Barra, A.-L.; Ramasesha, S.; Sutter, J.-P. Enhanced Ion Anisotropy by Nonconventional Coordination Geometry: Single-Chain Magnet Behavior for a $[\{Fe(II)L\}_2\{Nb(IV)(CN)_8\}]$ Helical Chain Compound Designed with Heptacoordinate Fe(II). *J. Am. Chem. Soc.* **2010**, *132* (17), 6047-6056. DOI: <https://doi.org/10.1021/ja9089389>.
- (19) Shao, D.; Zhang, S.-L.; Zhao, X.-H.; Wang, X.-Y. Spin canting, metamagnetism, and single-chain magnetic behaviour in a cyano-bridged homospin iron(II) compound. *Chem. Comm.* **2015**, *51* (21), 4360-4363. DOI: 10.1039/C4CC10003D.
- (20) Shao, D.; Zhao, X.-H.; Zhang, S.-L.; Wu, D.-Q.; Wei, X.-Q.; Wang, X.-Y. Structural and magnetic tuning from a field-induced single-ion magnet to a single-chain magnet by anions. *Inorg. Chem. Front.* **2015**, *2* (9), 846-853. DOI: 10.1039/C5QI00089K.
- (21) Pichon, C.; Suaud, N.; Duhayon, C.; Guihéry, N.; Sutter, J.-P. Cyano-Bridged Fe(II)–Cr(III) Single-Chain Magnet Based on Pentagonal Bipyramid Units: On the Added Value of Aligned Axial Anisotropy. *J. Am. Chem. Soc.* **2018**, *140* (24), 7698-7704. DOI: 10.1021/jacs.8b03891.
- (22) Drahoš, B.; Herchel, R.; Trávníček, Z. Single-Chain Magnet Based on 1D Polymeric Azido-Bridged Seven-Coordinate Fe(II) Complex with a Pyridine-Based Macrocyclic Ligand. *Inorg. Chem.* **2018**, *57* (20), 12718-12726. DOI: 10.1021/acs.inorgchem.8b01798.
- (23) Bretosh, K.; Béreau, V.; Duhayon, C.; Pichon, C.; Sutter, J.-P. A ferromagnetic Ni(II)–Cr(III) single-chain magnet based on pentagonal bipyramidal building units. *Inorg. Chem. Front.* **2020**, *7* (7), 1503-1511. DOI: 10.1039/C9QI01489F.
- (24) Aston, K.; Rath, N.; Naik, A.; Slomczynska, U.; Schall, O. F.; Riley, D. P. Computer-Aided Design (CAD) of Mn(II) Complexes: Superoxide Dismutase Mimetics with Catalytic Activity Exceeding the Native Enzyme. *Inorg. Chem.* **2001**, *40* (8), 1779-1789. DOI: 10.1021/ic000958v.
- (25) Drew, M. G.; Bin Othman, H.; Hill, W.; McIlroy, P.; Nelson, S. M. Seven-coordinate complexes of iron(II) with pentadentate macrocyclic ligands. *Inorg. Chim. Acta* **1975**, *12*, L25-L26. DOI: [https://doi.org/10.1016/S0020-1693\(00\)89819-9](https://doi.org/10.1016/S0020-1693(00)89819-9).
- (26) Bishop, M. M.; Lewis, J.; O'Donoghue, T. D.; Raithby, P. R.; Ramsden, J. N. X-Ray crystal structure of a planar, high-spin iron(II) complex of a pentadentate unsaturated macrocycle formed by reaction of 2,9-di(1-methylhydrazino)1,10-phenanthroline monohydrochloride with 2,6-diacetylpyridine. *J. Chem. Soc. Chem. Comm.* **1978**, *19*, 828-829. DOI: 10.1039/C39780000828.
- (27) Alvarez, S.; Alemany, P.; Casanova, D.; Cirera, J.; Llunell, M.; Avnir, D. Shape maps and polyhedral interconversion paths in transition metal chemistry. *Coord. Chem. Rev.* **2005**, *249* (17-18), 1693-1708. DOI: <https://doi.org/10.1016/j.ccr.2005.03.031>.
- (28) *SHAPE: Program for the stereochemical analysis of molecular fragments by means of continuous shape measures and associated tools*; University of Barcelona: Barcelona, 2013. http://www.ee.uib.edu/index.php?option=com_jdownloads&Itemid=529&view=viewcategory&catid=4.
- (29) Casanova, D.; Alemany, P.; Bofill, J. M.; Alvarez, S. Shape and symmetry of heptacoordinated transition-metal complexes: structural trends. *Chem. Eur. J.* **2003**, *9*, 1281-1295. DOI: <https://doi.org/10.1002/chem.200390145>.
- (30) Chilton, N. F.; Anderson, R. P.; Turner, L. D.; Soncini, A.; Murray, K. S. PHI. *J. Comput. Chem.* **2013**, *34*, 1164 – 1175. DOI: <https://doi.org/10.1002/jcc.23234>.
- (31) Bar, A. K.; Gogoi, N.; Pichon, C.; Goli, V. M. L. D. P.; Thlijeni, M.; Duhayon, C.; Suaud, N.; Guihéry, N.; Barra, A.-L.; Ramasesha, S.; et al. Pentagonal Bipyramid Fe(II) Complexes: Robust Ising-Spin Units towards Heteropolynuclear Nanomagnets. *Chem. Eur. J.* **2017**, *23* (18), 4380-4396. DOI: 10.1002/chem.201605549.
- (32) Drillon, M.; Coronado, E.; Beltran, D.; Georges, R. Classical treatment of a Heisenberg linear chain with spin alternation; application to the MnNi(EDTA)-6H₂O complex. *Chem. Phys.* **1983**, *79* (3), 449-453. DOI: [https://doi.org/10.1016/0301-0104\(83\)85267-7](https://doi.org/10.1016/0301-0104(83)85267-7).

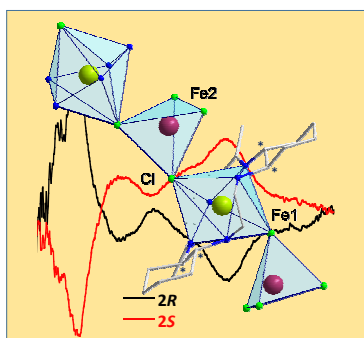
- (33) Georges, R.; Borrás-Almenar, J. J.; Coronado, E.; Curély, J.; Drillon, M. One-dimensional magnetism: An overview of the models. In *Magnetism: Molecules to materials: Models and experiments*, Miller, J.S. and Drillon, M. Ed.; Vol. 1; Wiley-VCH, 2002; pp 1-47. DOI: <https://doi.org/10.1002/3527600841.ch1>
- (34) Kahn, O. *Molecular Magnetism*; VCH, 1993.
- (35) Laskowski, E. J.; Felthouse, T. R.; Hendrickson, D. N.; Long, G. J. Magnetic exchange interactions in transition metal dimers. 8. Di- μ -chloro-bridged nickel(II) complexes. *Inorg. Chem.* **1976**, *15* (11), 2908-2911. DOI: 10.1021/ic50165a071.
- (36) Viñuelas-Zahinos, E.; Luna-Giles, F.; Torres-García, P.; Bernalte-García, A. Chloride-bridged Ni(II) complexes with ferromagnetic exchange interaction from thiazoline hydrazone derivative ligands. *Polyhedron* **2009**, *28* (7), 1362-1368. DOI: <https://doi.org/10.1016/j.poly.2009.02.030>.
- (37) Lhotel, E.; Khatsko, E. N.; Paulsen, C. Resonant quantum tunneling of spin chains in a three-dimensional magnetically ordered state. *Phys. Rev. B* **2006**, *74*, 020402. DOI: 10.1103/PhysRevB.74.020402.
- (38) Ishii, N.; Okamura, Y.; Chiba, S.; Nogami, T.; Ishida, T. Giant coercivity in one-dimensional cobalt-radical coordination magnet. *J. Am. Chem. Soc.* **2008**, *130*, 24-25. DOI: <https://doi.org/10.1021/ja077666e>.
- (39) Coulon, C.; Clérac, R.; Wernsdorfer, W.; Colin, T.; Miyasaka, H. Realization of a Magnet Using an Antiferromagnetic Phase of Single-Chain Magnets. *Phys. Rev. Lett.* **2009**, *102* (16), 167204. DOI: 10.1103/PhysRevLett.102.167204.
- (40) Werner, J.; Tomkowicz, Z.; Rams, M.; Ebbinghaus, S. G.; Neumann, T.; Näther, C. Synthesis, structure and properties of $[\text{Co}(\text{NCS})_2(4\text{-}(4\text{-chlorobenzyl)pyridine})_2]_n$, that shows slow magnetic relaxations and a metamagnetic transition. *Dalton Trans.* **2015**, *44* (31), 14149-14158. DOI: 10.1039/C5DT01898F.
- (41) Zhao, X.-H.; Deng, L.-D.; Zhou, Y.; Shao, D.; Wu, D.-Q.; Wei, X.-Q.; Wang, X.-Y. Slow Magnetic Relaxation in One-Dimensional Azido-Bridged Co(II) Complexes. *Inorg. Chem.* **2017**, *56* (14), 8058-8067. DOI: 10.1021/acs.inorgchem.7b00736.
- (42) Mautner, F. A.; Traber, M.; Fischer, R. C.; Torvisco, A.; Reichmann, K.; Speed, S.; Vicente, R.; Massoud, S. S. Synthesis and structural characterization of isothiocyanato-4-methoxypyridine-cobalt(II) complexes with diverse geometries and a bridged 1D coordination polymer showing metamagnetic transition. *Polyhedron* **2018**, *154*, 436-442. DOI: <https://doi.org/10.1016/j.poly.2018.08.022>.
- (43) Rams, M.; Jochim, A.; Böhme, M.; Lohmiller, T.; Ceglarska, M.; Rams, M. M.; Schnegg, A.; Plass, W.; Näther, C. Single-Chain Magnet Based on Cobalt(II) Thiocyanate as XXZ Spin Chain. *Chem. Eur. J.* **2020**, *26* (13), 2837-2851. DOI: 10.1002/chem.201903924.
- (44) Maurice, R.; Bastardis, R.; Graaf, C. d.; Suaud, N.; Mallah, T.; Guihéry, N. Universal Theoretical Approach to Extract Anisotropic Spin Hamiltonians. *J. Chem. Theo. Comput.* **2009**, *5* (11), 2977-2984. DOI: 10.1021/ct900326e.
- (45) Antal, P.; Drahoš, B.; Herchel, R.; Trávníček, Z. Structure and Magnetism of Seven-Coordinate Fe(III), Fe(II), Co(II) and Ni(II) Complexes Containing a Heptadentate 15-Membered Pyridine-Based Macrocyclic Ligand. *Eur. J. Inorg. Chem.* **2018**, (38), 4286-4297. DOI: 10.1002/ejic.201800769.
- (46) Mondal, A.; Wu, S.-Q.; Sato, O.; Konar, S. Effect of Axial Ligands on Easy-Axis Anisotropy and Field-Induced Slow Magnetic Relaxation in Heptacoordinated Fe(II) Complexes. *Chem. Eur. J.* **2020**, *26* (21), 4780-4789. DOI: 10.1002/chem.201905166.
- (47) Pichon, C.; Suaud, N.; Jubault, V.; Duhayon, C.; Guihéry, N.; Sutter, J.-P. Trinuclear Cyanido-Bridged $[\text{Cr}_2\text{Fe}]$ Complexes: To Be or not to Be a Single-Molecule Magnet, a Matter of Straightness. *Chem. Eur. J.* **2021**, *27* (62), 15484-15495. DOI: <https://doi.org/10.1002/chem.202102571>.

- (48) Ruamps, R.; Maurice, R.; de Graaf, C.; Guihéry, N. Interplay between Local Anisotropies in Binuclear Complexes. *Inorg. Chem.* **2014**, *53* (9), 4508-4516. DOI: 10.1021/ic500180k.
- (49) Betteridge, P. W.; Carruthers, J. R.; Cooper, R. I.; Prout, K.; Watkin, D. J. CRYSTALS version 12: software for guided crystal structure analysis. *J. Appl. Cryst.* **2003**, *36* (6), 1487. DOI: doi:10.1107/S0021889803021800.
- (50) Schmitz, W. International Tables for X-ray Crystallography, vol. IV (Ergänzungsband). Herausgegeben von der International Union of Crystallography. The Kynoch Press, Birmingham, England, 1974, 366 Seiten einschließlich Tabellen und Sachwortverzeichnis. *Krist. Tech.* **1975**, *10* (11), K120-K120. DOI: 10.1002/crat.19750101116.
- (51) Neese, F. The ORCA program system. *Wiley Inter. Rev.: Comput. Mol. Sci.* **2012**, *2* (1), 73-78. DOI: 10.1002/wcms.81.
- (52) Neese, F. Software update: the ORCA program system, version 4.0. *WIREs Comput. Mol. Sci.* **2018**, *8* (1), e1327. DOI: <https://doi.org/10.1002/wcms.1327>.
- (53) Perdew, J. P.; Burke, K.; Ernzerhof, M. Generalized Gradient Approximation Made Simple. *Phys. Rev. Lett.* **1996**, *77* (18), 3865-3868. DOI: 10.1103/PhysRevLett.77.3865.
- (54) Weigend, F.; Ahlrichs, R. Balanced basis sets of split valence, triple zeta valence and quadruple zeta valence quality for H to Rn: Design and assessment of accuracy. *Phys. Chem. Chem. Phys.* **2005**, *7* (18), 3297-3305. DOI: 10.1039/B508541A.
- (55) Chai, J.-D.; Head-Gordon, M. Long-range corrected hybrid density functionals with damped atom-atom dispersion corrections. *Phys. Chem. Chem. Phys.* **2008**, *10* (44), 6615-6620. DOI: 10.1039/B810189B.
- (56) David, G.; Guihéry, N.; Ferré, N. What Are the Physical Contents of Hubbard and Heisenberg Hamiltonian Interactions Extracted from Broken Symmetry DFT Calculations in Magnetic Compounds? *J. Chem. Theo. Comput.* **2017**, *13* (12), 6253-6265. DOI: 10.1021/acs.jctc.7b00976.
- (57) Angeli, C.; Cimiraglia, R.; Evangelisti, S.; Leininger, T.; Malrieu, J.-P. Introduction of n-electron valence states for multireference perturbation theory. *J. Chem. Phys.* **2001**, *114* (23), 10252-10264. DOI: <http://dx.doi.org/10.1063/1.1361246>.
- (58) Neese, F. Efficient and accurate approximations to the molecular spin-orbit coupling operator and their use in molecular g-tensor calculations. *J. Chem. Phys.* **2005**, *122* (3), 034107. DOI: 10.1063/1.1829047.
- (59) Bloch, C. Sur la théorie des perturbations des états liés. *Nucl. Phys.* **1958**, *6*, 329-347. DOI: [http://dx.doi.org/10.1016/0029-5582\(58\)90116-0](http://dx.doi.org/10.1016/0029-5582(58)90116-0).
- (60) des Cloizeaux, J. Extension d'une formule de Lagrange à des problèmes de valeurs propres. *Nucl. Phys.* **1960**, *20*, 321-346. DOI: [http://dx.doi.org/10.1016/0029-5582\(60\)90177-2](http://dx.doi.org/10.1016/0029-5582(60)90177-2).

For Table of Contents Use Only

Homochiral SCM built of tetrahedral and pentagonal bipyramidal Fe(II) units bridged by chlorine

Valentin Jubault,^a Barthélémy Pradines,^b Céline Pichon,^{a,*} Nicolas Suaud,^{b,*} Carine Duhayon,^a Nathalie Guihéry,^{b,*} Jean-Pascal Sutter^{a,*}



A chiral SCM consisting of alternating pentagonal bipyramidal Fe^{II} and tetrahedral [FeCl₄]²⁻ units bridged by Cl-atoms was found to exhibit a canted antiferromagnetic ordering with SCM behavior. The chiral pool is provided by an enantiopure macrocyclic pentadentate ligand.

Homochiral SCM built of tetrahedral and pentagonal bipyramidal Fe(II) units bridged by chlorine

Valentin Jubault,^a Barthélémy Pradines,^b Céline Pichon,^{a,*} Nicolas Suaud,^{b,*} Carine Duhayon,^a Nathalie Guihéry,^{b,*} Jean-Pascal Sutter^{a,*}

^a Laboratoire de Chimie de Coordination du CNRS (LCC), Université de Toulouse, CNRS, F-31077 Toulouse, France.

e-mail : jean-pascal.sutter@lcc-toulouse.fr ; celine.pichon@lcc-toulouse.fr

^b Laboratoire de Chimie et Physique Quantiques (LCPQ), Université de Toulouse, CNRS, 118 route de Narbonne, F-31062 Toulouse, France.

e-mail: suaud@irsamc.ups-tlse.fr ; nathalie.guihery@irsamc.ups-tlse.fr

CONTENT

Synthetic procedures

Table S1. Crystallographic data for **1R**, **1S**, **2R**, and **2S**.

Table S2. Results of the analyses of the coordination polyhedra by SHAPE for **1R**, **1S**, **2R**, and **2S**.

Figure S1. Experimental (in black) and calculated (in blue) powder X-ray diffraction (PXRD) patterns for bulk samples of (from a to d) **1R**, **1S**, **2R**, **2S**.

Figure S2. Asymmetric unit with atoms' label of the crystal structures of **1R** and **1S** with ellipsoids are drawn at 30 % probability level, and selected bond distances (Å) and angles (°).

Figure S3. Asymmetric unit with atoms' label of the crystal structures of **2R** and **2S** with ellipsoids are drawn at 30 % probability level, and selected bond distances (Å) and angles (°). * = 1-x,1-y,1.5-z.

Figure S4. Solid state CD spectra for **1R** (in black), and **1S** (in red) (about 1 %mass in KBr pellets).

Figure S5. Magnetic behaviors for [FeL^{N5R,R}{FeCl₄}], **2R** : (a) Field-cooled (FC), zero-field cooled (ZFC), and remanant magnetization recorded with H_{DC} = 10 Oe ; (b) M versus H behaviors between 2 and 8 K

Figure S6: AC magnetic susceptibility for [FeL^{N5R,R}{FeCl₄}], **2R** :

Figure S7. Fragments either centered on [FeCl₄]²⁻ (F1 in a) or [FeL^{N5R,R}}²⁺ (F2 in b) complexes. The Fe^{II} ions located on the borders in the real compound have been replaced by Zn^{II} ions (in grey) for the calculation of magnetic couplings.

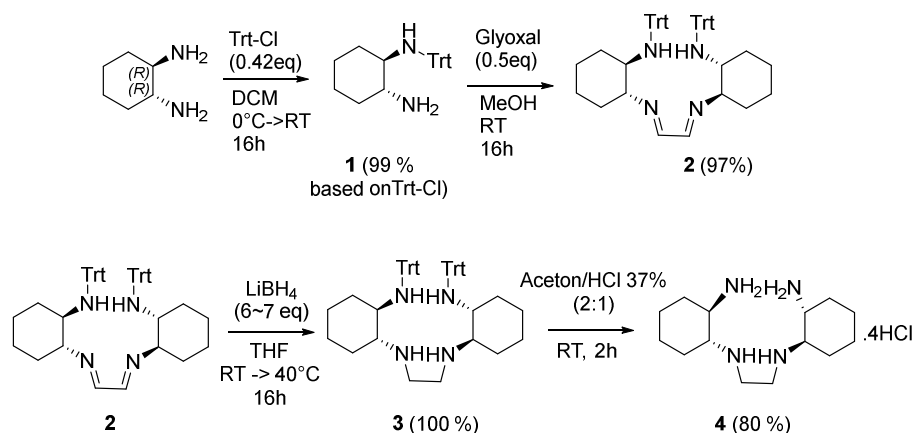
Figure S8. Additional views of the calculated magnetic axes (x in red, y in green, and z in blue) for the Fe^{II} centers in 1-D [FeL^{N5R,R}{FeCl₄}], **2R**.

REFERENCES

Synthetic procedures:

N,N'-Bis{(1*R*,2*R*)-[2-(amino)]cyclohexyl}-1,2-diaminoethane tetrachlorhydrate:

The synthesis of this molecule was adapted from a reported procedure,¹ and illustrated in Scheme S1. The related *S*-enantiomer was obtained following same procedure but starting with (1*S*,2*S*)-1,2-diaminocyclohexane.



Scheme S1. Synthesis-pathway for the preparation of the tetra-amines illustrated with the *R*-enantiomer.

Step 1: N-(triphenylmethyl)-(1*R*,2*R*)-diaminocyclohexane, **1R**: Under inert atmosphere, (1*R*,2*R*)-1,2-diaminocyclohexane (25 g, 219.25 mmol) transferred in an 1 liter two-neck balloon was dissolved in 350 mL of dried DCM. Triphenylmethyl chloride (25.7 g, 92.09 mmol) dissolved in 200 mL of dried DCM was added dropwisely over 30 min at 0°C. The reaction medium was heated at 30°C during 16 h. The pale yellow solution was checked by ¹³C NMR to follow the reaction. When all the triphenylmethyl chloride reacted, the peak at 80 ppm disappeared. Once the reaction was complete, the mixture was washed with 4 x 200 mL of distilled water or until the pH was below 8. The organic phase was dried over Na₂SO₄ before evaporation to dryness with a rotary evaporator giving a sticky pale yellow solid which after 2 hours under vacuum with a Schlenk line gave a well-dried foam. Yield : 32.2 g (99 %). ¹H NMR (400 MHz, CDCl₃) δ (ppm) : 7.71 (d, 6 H, H_{aro}), 7.35 (t, 6 H, H_{aro}), 7.25 (t, 3 H, H_{aro}), 2.62 (dt, 1 H, CH_{cyclohex}), 1.90-0.87 (m, 10 H, CH_{cyclohex}, CH_{2 cyclohex}, NH); NMR ¹³C {¹H} (400 MHz, CDCl₃) δ (ppm) : 147.52, 129.08, 127.65, 126.15, 70.78, 59.46, 55.37, 37.08, 33.26, 25.06, 24.88.

Step 2: Glyoxal bisimine of N-(triphenylmethyl)-(1*R*, 2*R*)-diaminocyclohexane, **2R**: The pale yellow solid obtained step 1 (32.25 g; 90.5 mmol) is dissolved in 400 mL MeOH before adding dropwisely glyoxal solution 40 % (5.19 mL, 45.25 mmol) at room temperature. The solution quickly turned troubled before a white solid massively precipitated. The reaction mixture was mixed at 30°C during 16 hours before Büchner filtration to collect the white solid from the orange filtrate. The solid was washed three times in MeOH (40 mL) by dispersion followed by filtration. After drying under vacuum, a white powder was obtained. Yield = 32 g (96 %). RMN ¹H (400 MHz, CDCl₃) δ (ppm) : 7.91 (s, 1 H, CH_{imine}), 7.55 (d, 6 H, H_{aro}), 7.18-7.10 (m, 9 H, H_{aro}), 3.02-2.97 (m, 1 H, CH_{cyclohex}), 2.47-2.42 (m, 1 H, CH_{cyclohex}), 1.95 (s, 1 H, NH), 1.66-1.60 (m, 2 H, CH_{2 cyclohex}), 1.46-1.39 (m, 2 H, CH_{2 cyclohex}), 1.32-1.21 (m, 2 H, CH_{2 cyclohex}), 1.01-0.91 (m, 2 H, CH_{2 cyclohex}); NMR ¹³C {¹H} (400 MHz, CDCl₃) δ (ppm) : 161.70, 147.23, 128.90, 127.63, 126.17, 73.76, 70.84, 56.73, 32.48, 31.78, 24.04, 23.61.

Step 3: N,N'-Bis{(1*R*,2*R*)-[2-(triphenylmethylamino)]cyclohexyl}-1,2-diaminoethane **3R**: The compound obtained step 2 (32 g, 43.6 mmol) was dissolved in 300 mL anhydrous THF under inert

atmosphere. A solution of LiBH_4 4 M in THF (54 mL, 218 mmol, 5 eq.) was dropwisely added at room temperature to the homogeneous pale yellow solution. A slight gaseous emission was noticed along with a solution discoloration and a trouble formation. The reaction mixture was heated to 40° C during 20 hours and the reaction progression was monitored by ^1H NMR following the disappearance of the imino proton at 7.91 ppm. On the basis of a NMR spectrum performed on the raw material, the conversion was around 95 %. 1 equivalent of LiBH_4 was then added and the reaction was let to proceed at room temperature during 16 hours. The LiBH_4 excess was carefully neutralized with 55 mL of distilled water before full evaporation of THF. The obtained white pasty solid was worked up in 165 mL DCM and 55 mL distilled water and this mixture was transferred in a separating funnel. The organic phase was collected and the aqueous phase was extracted with 2 x 50 mL of DCM. The organic phases were dried with Na_2SO_4 before evaporation to dryness under Schlenk vacuum during few hours giving a white powder. Yield = 30.28 g (94 %).

Step 4: N,N'-Bis{(1R,2R)-[2-(amino)]cyclohexyl}-1,2-diaminoethane tetrachlorhydrate **4R**: The deprotection of N,N'-Bis{(1R,2R)-[2-(triphenylmethylamino)]cyclohexyl}-1,2-diaminoethane (30.3 g, 41.1 mmol) was made in a mixture acetone/concentrated HCl (150 mL/75 mL) heating at 30°C during 4 hours. An intense yellow color, characteristic of the intermediate tritylcarbenium cation, quickly appeared before fading away leading to a white suspension. The solvents are evaporated to dryness until the isolation of a viscous solid. This product was fully dried with 100 mL of $\text{Et}_2\text{O}/\text{MeOH}$ 8:2. The resulting fine powder was filtered and washed with 3 x 100 mL Et_2O to remove the remaining triphenylmethanol. The white powder was fully dried under vacuum during 2 hours. Yield = 74 % (12 g). ^1H NMR (400 MHz, DMSO-d^6) : δ (ppm) 10.13 (s, 4 H, NH_2^+), 8.77 (s, 6 H, NH_3^+), 3.69-3.42 (m, 8 H, CH_2 cyclohex), 2.16 (t, 4 H, $-\text{CH}_2$ ethane-diamine), 1.75-1.49 (m, 8 H, $-\text{CH}_2$ cyclohex), 1.27-1.20 (ddd, 4 H, $-\text{CH}$ cyclohex) ; RMN ^{13}C $\{^1\text{H}\}$ (100 MHz, DMSO-d^6) : δ (ppm) 58.20, 50.60, 40.96, 29.11, 26.30, 22.84, 22.59. Elemental analysis (%) calculated for $\text{C}_{14}\text{H}_{34}\text{Cl}_4\text{N}_7$: C 42.01; H 8.56; N 14.00; experimental: C 41.91; H 8.28; N 13.64.

Table S1. Crystallographic data for **1R**, **1S**, **2R**, and **2S**.

	1S	1R	2S	2R
Chemical formula	C ₂₄ H ₄₁ Cl ₂ FeN ₅ O ₂	C ₂₄ H ₄₁ Cl ₂ Fe N ₅ O ₂	C ₂₃ H ₃₅ Cl ₄ Fe ₂ N ₅	C ₂₃ H ₃₅ Cl ₄ Fe ₂ N ₅
M (g.mol ⁻¹)	558.37	558.37	635.07	635.07
Crystal system	Orthorhombic	Orthorhombic	Tetragonal	Tetragonal
Space group	<i>P</i> 2 ₁ 2 ₁ 2 ₁	<i>P</i> 2 ₁ 2 ₁ 2 ₁	<i>P</i> 4 ₁ 2 ₁ 2	<i>P</i> 4 ₃ 2 ₁ 2
a (Å)	8.2281(1)	8.2115(6)	12.7230(6)	12.7282(1)
b (Å)	17.5055(2)	17.574(2)	12.7230(6)	12.7282(1)
c (Å)	18.6548(2)	18.636(2)	16.9681(8)	16.9617(2)
α (°)	90	90	90	90
β (°)	90	90	90	90
γ (°)	90	90	90	90
V (Å ³)	2686.98(5)	2689.3(4)	2746.7(3)	2747.92(5)
Z	4	4	4	4
d _{calc}	1.380	1.379	1.536	1.535
λ (Å)	1.54180 (Cu Kα)	0.71073 (Mo Kα)	0.71073 (Mo Kα)	1.54180 (Cu Kα)
μ (mm ⁻¹)	6.571	0.790	1.467	12.215
T (K)	100	100	100	100
Refl. measured	122218	65515	77605	28854
Refl. unique	5578	6756	3407	2961
R _{int}	0.058	0.047	0.058	0.033
Refinement on	F ²	F	F ²	F ²
Refl. with I > 2σ(I)	5049	6563	3352	2912
Nb. parameters	308	308	147	159
R with I > 2σ(I)	0.0220	0.0248	0.0418	0.0309
R _w with I > 2σ(I)	0.0564	0.0269	0.0955	0.0762
Flack parameter	-0.009(2)	0.021(8)	0.046(5)	-0.0002(15)
Residual electron density (e ⁻ .Å ⁻³)	0.21/-0.16	0.51/-0.38	0.46/-0.43	0.39/-0.43
CCDC reference	2214580	2214581	2214582	2214583

Table S2. Results of the analyses of the coordination polyhedra by SHAPE for **1R**, **1S**, **2R**, and **2S**.

FeL₇	PBPY-7	COC-7	CTPR-7	JPBPY-7	JETBPY-7
1R	0.493	6.872	5.237	4.536	22.899
1S	0.543	6.916	5.187	4.522	22.472
2R	2.014	4.791	3.483	8.320	22.923
2S	1.500	5.572	4.283	7.792	22.903
FeCl₄	SP-4	T-4	SS-4	vTBPY-4	
2R	24.358	1.152	6.712	3.978	
2S	24.271	1.165	6.684	3.991	

Reference geometries:

- PBPY-7 (D_{5h}) Pentagonal bipyramid
COC-7 (C_{3v}) Capped octahedron
CTPR-7 (C_{2v}) Capped trigonal prism
JPBPY-7 (D_{5h}) Johnson pentagonal bipyramid J13
JETPY-7 (C_{3v}) Johnson elongated triangular pyramid J7
- SP-4 (D_{4h}) Square
T-4 (Td) Tetrahedron
SS-4 (C_{2v}) Seesaw
vTBPY-4 (C_{3v}) Vacant trigonal bipyramid

Figure S1. Experimental (in black) and calculated (in blue) powder X-ray diffraction (PXRD) patterns for bulk samples of (from a to d) **1R**, **1S**, **2R**, **2S**.

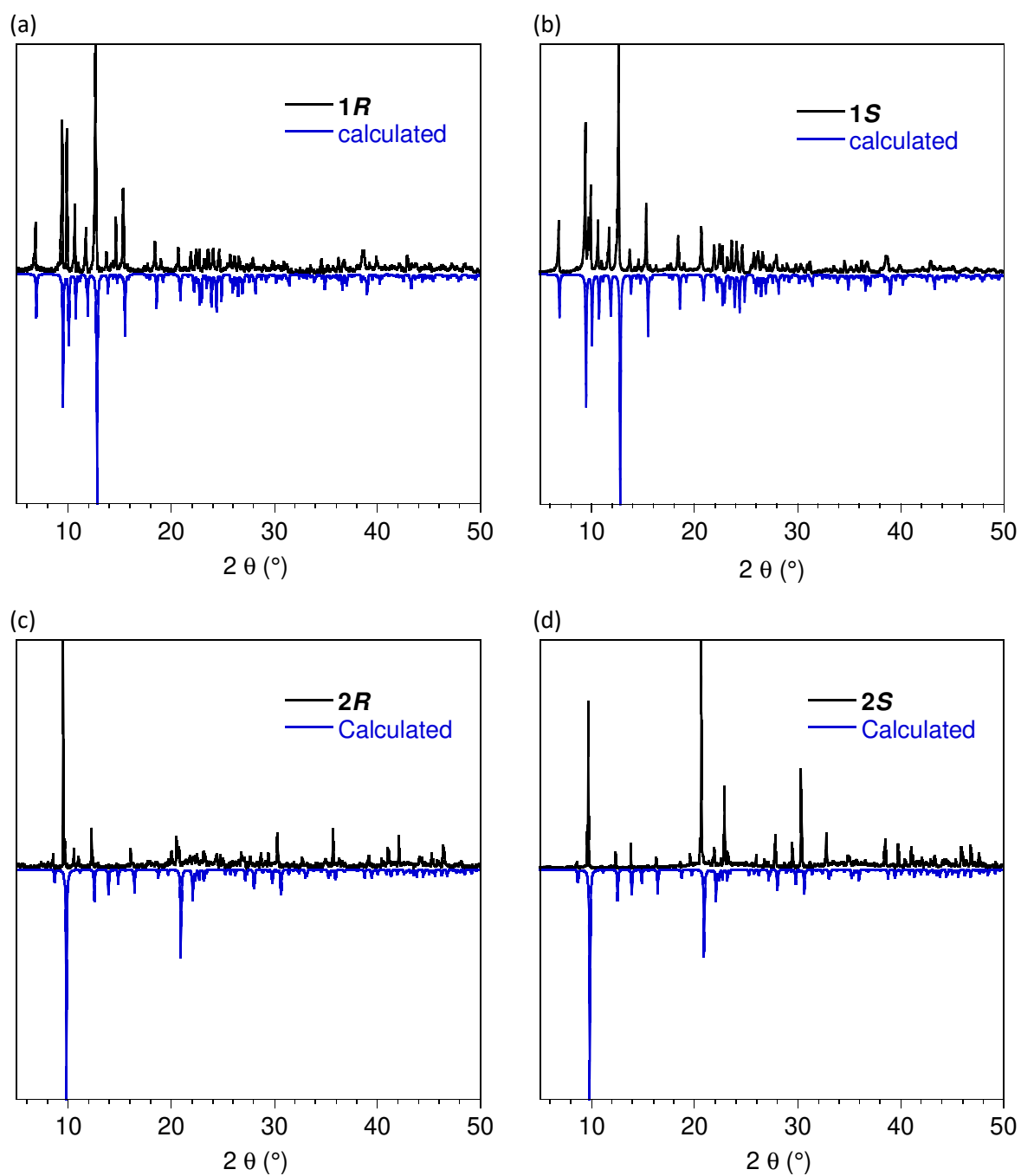
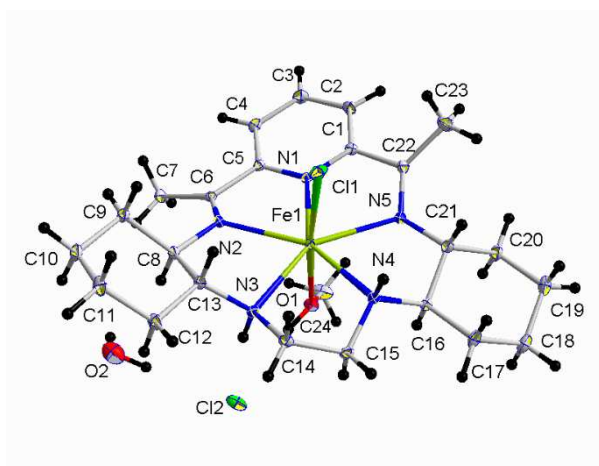


Figure S2. Asymmetric unit with atoms' label of the crystal structures of **1R** and **1S** with ellipsoids are drawn at 30 % probability level, and selected bond distances (Å) and angles (°).



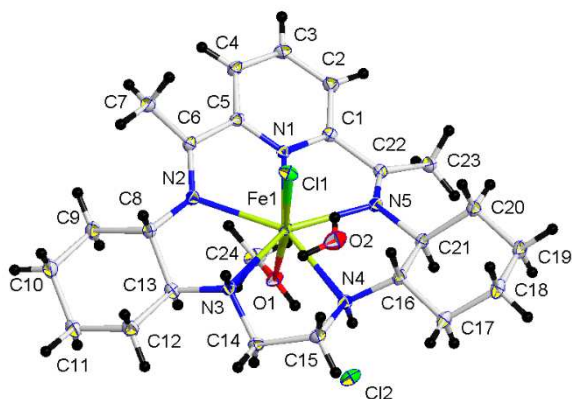
Distances (Å)

C1	C2	1.397(2)	C1	C22	1.495(2)
C1	N1	1.340(2)	C2	C3	1.392(2)
C5	N1	1.338(2)	C3	C4	1.393(2)
C6	N2	1.280(2)	C4	C5	1.393(2)
C8	C9	1.537(2)	C5	C6	1.494(2)
C8	N2	1.466(2)	C6	C7	1.492(2)
C9	C10	1.535(2)	C8	C13	1.536(2)
C11	C12	1.537(2)	C10	C11	1.527(2)
C13	N3	1.473(2)	C12	C13	1.529(2)
C14	C15	1.5164(19)	C14	N3	1.472(2)
C15	N4	1.471(2)	C16	C17	1.522(2)
C16	C21	1.532(2)	C16	N4	1.474(2)
C18	C19	1.530(2)	C17	C18	1.530(2)
C20	C21	1.534(2)	C19	C20	1.520(2)
C22	N5	1.300(2)	C21	N5	1.441(2)
C24	O1	1.4140(16)	C22	C23	1.479(2)
N1	Fe1	2.173(1)	N2	Fe1	2.282(1)

N3	Fe1	2.305(1)	Fe1	Cl1	2.4663(4)
N4	Fe1	2.262(1)	Fe1	O1	2.2007(9)
N5	Fe1	2.345(1)			

Angles (°)

N1	Fe1	N2	70.77(4)	N1	Fe1	N3	141.48(4)
N2	Fe1	N3	71.60(4)	N1	Fe1	N4	141.55(4)
N2	Fe1	N4	147.57(4)	N3	Fe1	N4	76.65(4)
N1	Fe1	N5	69.79(4)	N2	Fe1	N5	140.55(4)
N3	Fe1	N5	147.24(4)	N4	Fe1	N5	71.82(4)
N1	Fe1	Cl1	90.04(3)	N2	Fe1	Cl1	92.45(3)
N3	Fe1	Cl1	99.51(3)	N4	Fe1	Cl1	86.28(3)
N5	Fe1	Cl1	87.26(3)	N1	Fe1	O1	90.59(4)
N2	Fe1	O1	92.41(4)	N3	Fe1	O1	83.02(4)
N4	Fe1	O1	90.16(4)	N5	Fe1	O1	88.32(4)
Cl1	Fe1	O1	175.02(3)	C24	O1	Fe1	125.06(9)



1S

Distances (Å)

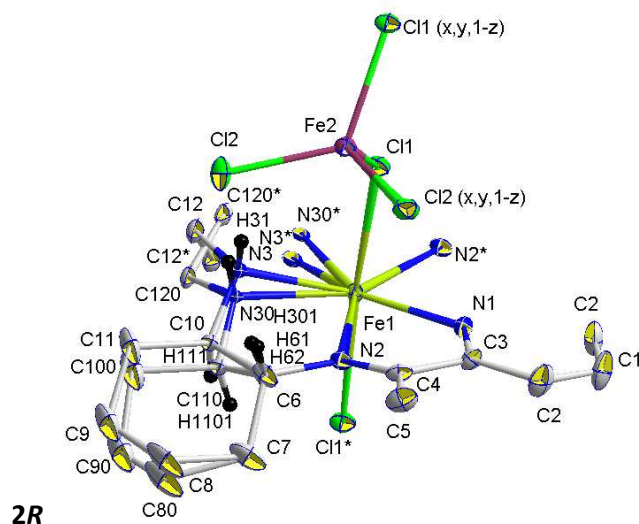
Fe1	Cl1	2.4653(5)	Fe1	N1	2.1697(13)
Fe1	N2	2.3524(13)	Fe1	N3	2.2601(14)
Fe1	N4	2.3017(13)	Fe1	N5	2.2795(14)
Fe1	O1	2.1850(11)	C1	C2	1.395(2)
C1	C22	1.493(2)	C1	N1	1.337(2)
C2	C3	1.390(2)	C5	N1	1.344(2)
C3	C4	1.387(3)	C6	N2	1.288(2)
C4	C5	1.394(2)	C8	C9	1.535(2)
C5	C6	1.487(2)	C8	N2	1.463(2)
C6	C7	1.493(2)	C9	C10	1.524(3)
C8	C13	1.528(2)	C11	C12	1.527(2)
C10	C11	1.526(3)	C13	N3	1.477(2)
C12	C13	1.520(2)	C14	C15	1.512(2)
C14	N3	1.474(2)	C15	N4	1.467(2)
C16	C17	1.529(2)	C16	C21	1.529(2)
C16	N4	1.477(2)	C18	C19	1.521(3)
C17	C18	1.531(3)	C20	C21	1.540(2)

C19	C20	1.530(2)	C22	N5	1.278(2)
C21	N5	1.468(2)	C24	O1	1.421(2)
C22	C23	1.491(2)			

Angles (°)

Cl1	Fe1	N1	88.95(4)	Cl1	Fe1	N2	86.26(4)
N1	Fe1	N2	69.58(5)	Cl1	Fe1	N3	85.65(4)
N1	Fe1	N3	141.50(5)	N2	Fe1	N3	72.03(5)
Cl1	Fe1	N4	100.51(4)	N1	Fe1	N4	141.59(5)
N2	Fe1	N4	147.42(5)	N3	Fe1	N4	76.72(5)
Cl1	Fe1	N5	93.06(4)	N1	Fe1	N5	70.58(5)
N2	Fe1	N5	140.17(5)	N3	Fe1	N5	147.71(5)
N4	Fe1	N5	71.80(5)	Cl1	Fe1	O1	174.31(3)
N1	Fe1	O1	90.97(5)	N2	Fe1	O1	88.38(5)
N3	Fe1	O1	90.89(5)	N4	Fe1	O1	83.03(5)
N5	Fe1	O1	92.27(5)				

Figure S3. Asymmetric unit with atoms' label of the crystal structures of **2R** and **2S** with ellipsoids are drawn at 30 % probability level, and selected bond distances (Å) and angles (°). * = 1-x,1-y,1.5-z.

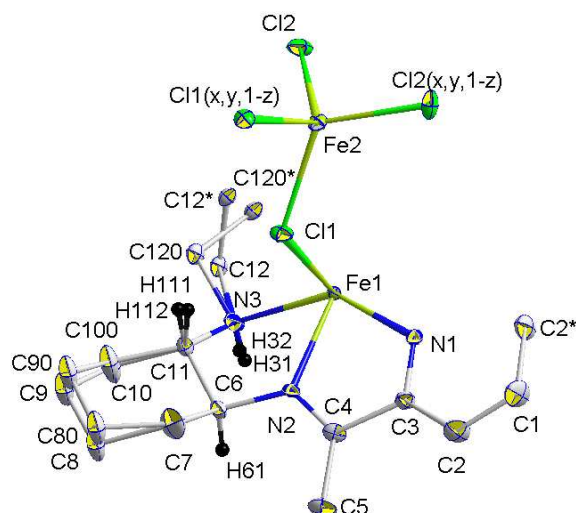


Distances (Å)

C1	C2	1.368(4)	C2	C3	1.388(4)
C3	N1	1.331(3)	C3	C4	1.495(4)
C4	N2	1.279(4)	C4	C5	1.502(4)
C6	C7	1.525(4)	C6	C11	1.617(5)
C6	N2	1.465(4)	C6	C110	1.354(4)
C7	C8	1.584(6)	C7	C80	1.555(6)
C8	C9	1.589(8)	C8	C90	1.606(9)
C8	C80	0.602	C9	C100	1.233(7)
C9	C10	1.485(8)	C9	C80	1.510(9)
C9	C90	0.697	C10	C11	1.539(4)
C10	C100	0.520	C10	C110	1.697(5)
C11	C100	1.505(4)	C11	N30	1.085(4)
C11	N3	1.471(4)	C11	C110	0.467
C12	N3	1.451(4)	C12	C120	0.876
Fe1	Cl1	2.5993(6)	C12	N30	1.656(4)
Fe1	N1	2.148(3)	Fe1	N2	2.242(2)
C120	N30	1.491(4)	Fe1	N30	2.258(2)
C100	C110	1.558(4)	Fe1	N3	2.262(2)
C90	C80	1.268(8)	Fe2	Cl1	2.3388(7)
N30	C110	1.437(4)	Fe2	Cl2	2.2939(7)
C100	C90	1.507(9)	C120	N3	1.558(4)

Angles (°);* = 1-x,1-y,1.5-z

Cl1	Fe1	N1	87.832(18)	Cl1	Fe1	Cl1*	175.66(4)
Cl1	Fe1	N2	95.97(6)	Cl1*	Fe1	N1	87.832(18)
N1	Fe1	N2	71.43(6)	Cl1*	Fe1	N2	82.64(6)
Cl1*	Fe1	N2*	95.97(6)	Cl1	Fe1	N2*	82.64(6)
N2	Fe1	N2*	142.86(12)	N1	Fe1	N2*	71.43(6)
Cl1*	Fe1	N30	91.30(8)	Cl1	Fe1	N30	92.01(8)
N2	Fe1	N30	68.66(9)	N1	Fe1	N30	139.85(7)
Cl1	Fe1	N30*	91.30(8)	N2*	Fe1	N30	148.28(9)
N1	Fe1	N30*	139.85(7)	Cl1*	Fe1	N30*	92.01(8)
N2*	Fe1	N30*	68.66(9)	N2	Fe1	N30*	148.28(9)
Cl1*	Fe1	N3	103.13(8)	Cl1	Fe1	N3	80.35(8)
N2	Fe1	N3	73.92(9)	N1	Fe1	N3	141.87(6)
Cl1	Fe1	N3*	103.13(8)	N2*	Fe1	N3	141.07(9)
N1	Fe1	N3*	141.87(6)	Cl1*	Fe1	N3*	80.35(8)
N2*	Fe1	N3*	73.92(9)	N2	Fe1	N3*	141.07(9)
N30	Fe1	N3	12.253(12)	N30	Fe1	N30*	80.29(13)
N30	Fe1	N3*	76.98(13)	N30*	Fe1	N3	76.98(13)
N3	Fe1	N3*	76.26(13)	N30*	Fe1	N3*	12.253(12)
Cl1	Fe2	Cl2	106.11(2)	Cl1	Fe2	Cl1(x,y,1-z)	96.02(4)
Cl1	Fe2	Cl2(x,y,1-z)	120.75(3)	Cl1(x,y,1-z)	Fe2	Cl2	120.75(3)
Cl2	Fe2	Cl2(x,y,1-z)	107.75(5)	Cl1(x,y,1-z)	Fe2	Cl2(x,y,1-z)	106.11(2)
				Fe1	Cl1	Fe2	122.63(3)



2S

Distances (Å)

C4	N2	1.277(5)		C6	C11	1.534(6)
C6	C7	1.534(6)		C6	H61	0.986
C6	N2	1.463(5)		C7	C80	1.464(7)
C7	C8	1.621(9)		C11	C100	1.478(6)
C11	N3	1.453(6)		N1	Fe1	2.146(4)
C11	C10	1.583(7)		N3	Fe1	2.257(3)
N2	Fe1	2.244(3)		N3	C12	1.508(6)
N3	C120	1.524(6)		Fe2	Cl1(x,y,1-z)	2.3386(9)
Fe2	Cl1	2.3386(9)		Fe2	Cl2(x,y,1-z)	2.296(1)
Fe2	Cl2	2.296(1)		C100	C9	1.137(9)
Cl1	Fe1	2.6006(8)		C90	C80	1.48(1)
C100	C90	1.48(1)		C9	C8	1.51(1)
C10	C9	1.51(1)		C90	C8	1.49(1)

Angles (°);* = 1-x,1-y,1.5-z

Cl1	Fe2	Cl2	105.93(3)		Cl1	Fe2	Cl1(x,y,1-z)	96.14(5)
Cl1	Fe2	Cl2(x,y,1-z)	120.85(4)		Cl1(x,y,1-z)	Fe2	Cl2	120.85(4)
Cl2	Fe2	Cl2(x,y,1-z)	107.81(6)		Cl1(x,y,1-z)	Fe2	Cl2(x,y,1-z)	105.93(3)
N1	Fe1	N2	71.52(8)		Fe2	Cl1	Fe1	122.62(4)
N2	Fe1	N2*	143.05(16)		N1	Fe1	N2*	71.52(8)
N2	Fe1	N3	72.12(12)		N1	Fe1	N3	141.43(9)
N1	Fe1	N3*	141.43(9)		N2*	Fe1	N3	143.39(12)
N2*	Fe1	N3*	72.12(12)		N2	Fe1	N3*	143.39(12)
N1	Fe1	Cl1	87.92(3)		N3	Fe1	N3*	77.13(17)
N2*	Fe1	Cl1	96.01(7)		N2	Fe1	Cl1	82.66(7)
N3*	Fe1	Cl1	83.48(11)		N3	Fe1	Cl1	99.80(11)
N2	Fe1	Cl1*	96.01(7)		N1	Fe1	Cl1*	87.92(3)
N3	Fe1	Cl1*	83.48(11)		N2*	Fe1	Cl1*	82.66(7)
Cl1	Fe1	Cl1*	175.84(5)		N3*	Fe1	Cl1*	99.80(11)

Figure S4. Solid state CD spectra for **1R** (in black), and **1S** (in red) (about 1 %mass in KBr pellets).

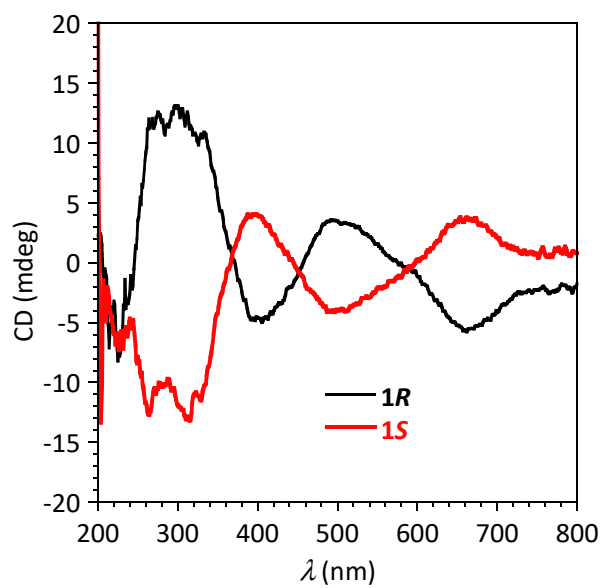


Figure S5. Magnetic behaviors for $[\text{FeL}^{\text{N5R,R}}\{\text{FeCl}_4\}]$, **2R**: (a) Field-cooled (FC), zero-field cooled (ZFC), and remanent magnetization recorded with $H_{\text{DC}} = 10$ Oe; (b) M versus H behaviors between 2 and 8 K; (c) $\chi_{\text{M}}T$ versus T obtained with $H = 1$ kOe: experimental (\square) and calculated ($-$), fit between 300 and 17 K, the part down to 2 K is an extrapolation); (d) $\chi_{\text{M}}T$ versus T between 25 and 2 K obtained for $H = 1000$ Oe, 25 Oe, and 10 Oe; (f) $\ln(\chi_{\text{M}}'T)$ versus $1/T$ recorded for $\nu = 1$ Hz.

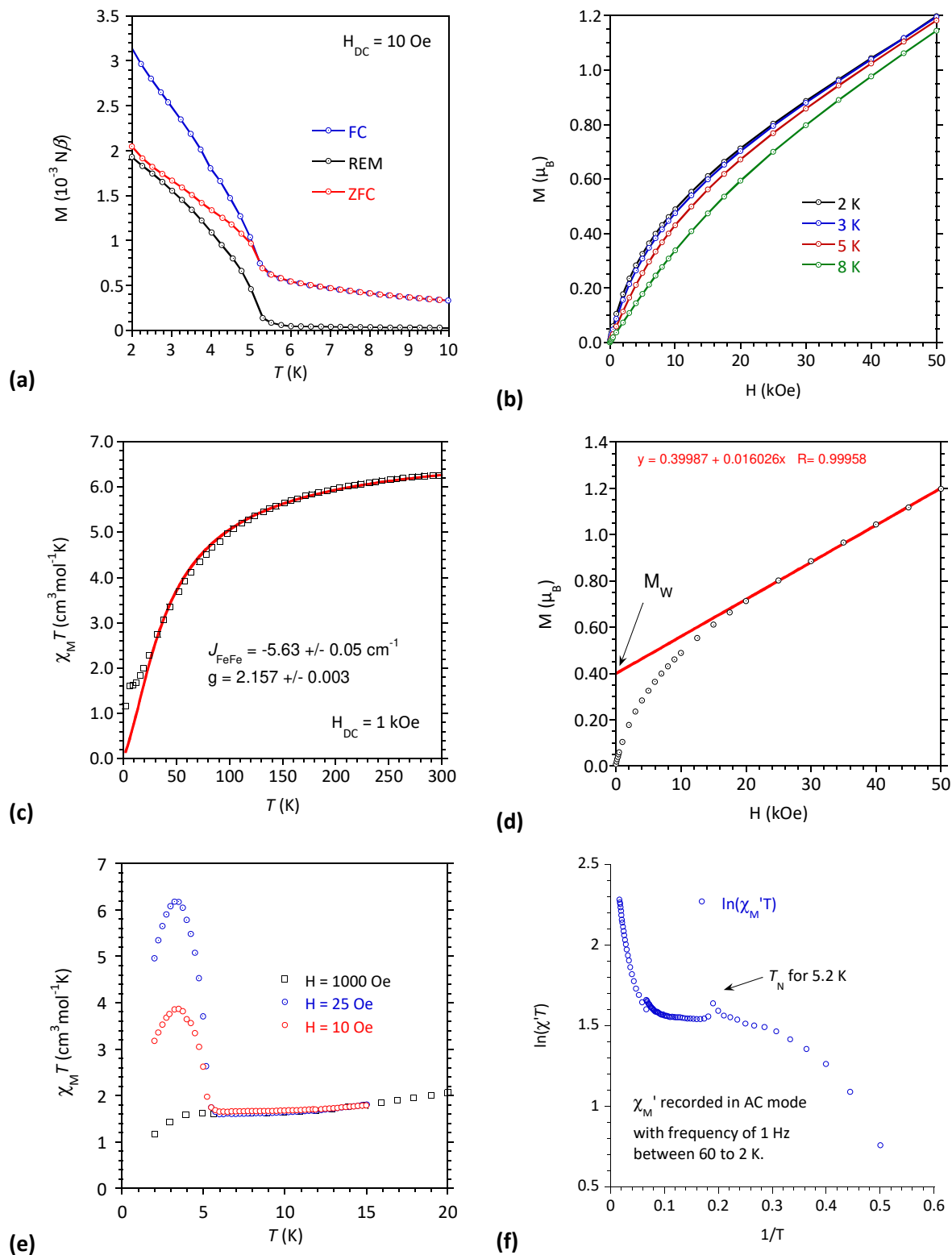
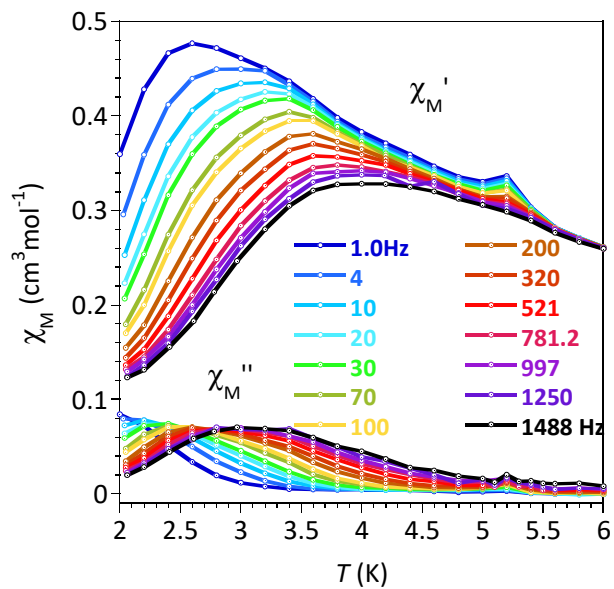


Figure S6: AC magnetic susceptibility for $[\text{FeL}^{\text{NSR,R}}\{\text{FeCl}_4\}]$, **2R** :

χ_M' and χ_M'' versus T for ν range 1 – 1488 Hz



χ_M'' versus ν for T between 2.0 and 4.2 K

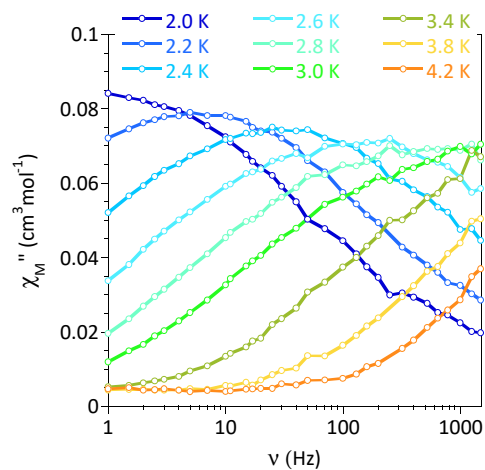
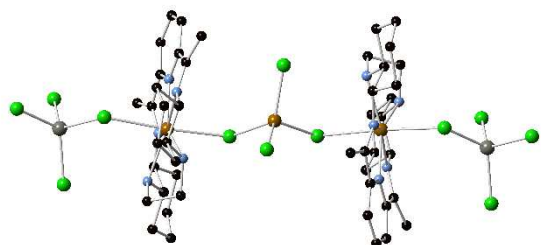


Figure S7. Fragments either centered on $[\text{FeCl}_4]^{2-}$ (F1 in a) or $[\text{FeL}^{\text{N}5\text{R},\text{R}}]^{2+}$ (F2 in b) complexes. The Fe^{II} ions located on the borders in the real compound have been replaced by Zn^{II} ions (in grey) for the calculation of magnetic couplings.

(a) fragment F1



(b) fragment F2

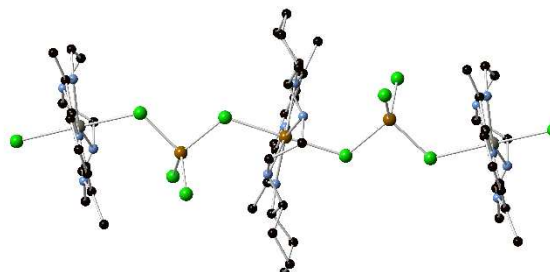
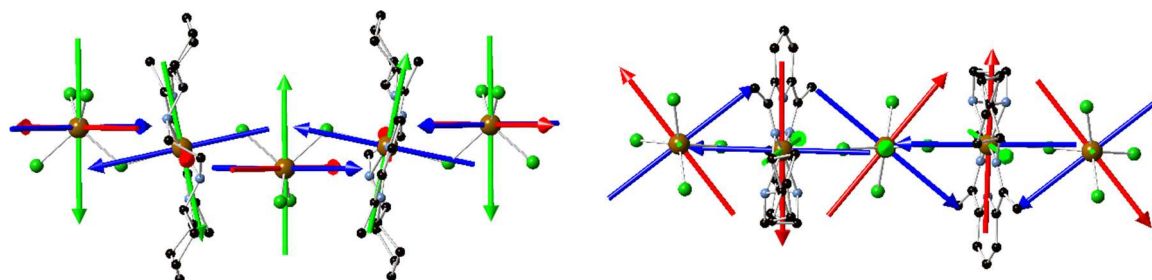


Figure S8. Additional views of the calculated magnetic axes (x in red, y in green, and z in blue) for the Fe^{II} centers in 1-D $[\text{FeL}^{\text{N}5\text{R},\text{R}}\{\text{FeCl}_4\}]$, **2R**.



REFERENCES

(1) Ornberg, R. L.; Udipi, K.; Forster, D.; Riley, D. P.; Thurmond, K. B.; Henke, S.; Brethauer, K.; Joardar, S. MODIFIED HYALURONIC ACID POLYMERS. US US 2004/0110722 A1, 2004.